

Article

Nitrate Absorption and Desorption by Biochar

Zijian He ¹, Chao Wang ¹, Hongxia Cao ^{1,*} , Jiaping Liang ^{2,*}, Shuyao Pei ¹ and Zhijun Li ¹

¹ Key Laboratory of Agricultural Soil and Water Engineering in Arid and Semiarid Areas, Ministry of Education, Northwest A&F University, Yangling 712100, China; hezj@nwfau.edu.cn (Z.H.); wangchao422@nwfau.edu.cn (C.W.); peisy@nwfau.edu.cn (S.P.); lizhij@nwsuaf.edu.cn (Z.L.)

² Faculty of Modern Agricultural Engineering, Kunming University of Science and Technology, Kunming 650500, China

* Correspondence: nschx225@nwfau.edu.cn (H.C.); liangjpxaut@163.com or 20210203@kust.edu.cn (J.L.)

Abstract: Biochar is a potential solution for addressing environmental problems related to excessive nitrogen (N). However, there is still some debate about the absorption and desorption of nitrate nitrogen (NO_3^- -N). Therefore, this study investigated the NO_3^- -N adsorption and desorption performance onto biochar and biochar-soil mixture to address this gap. The results showed that the biochar produced from apple branches had the ability to absorb NO_3^- -N with an absorption capacity of $3.51 \text{ mg}\cdot\text{g}^{-1}$. The absorption data fitted well with the pseudo-second-order kinetic model and Langmuir model. The application of biochar significantly improved soil absorption capacity and slow release of NO_3^- -N. While higher NO_3^- -N concentrations had better NO_3^- -N supply capacity and poorer slow-release effect. Integrating nutrient supply and slow-release effect, it is recommended to control the application ratio of biochar to NO_3^- -N at $34\text{--}42.75 \text{ g}\cdot\text{g}^{-1}$. Although the unoptimized biochar application rate cannot be directly applied to the soil as a slow-release fertilizer carrier to meet commercial standards, biochar modification provides new possibilities for this purpose. Moreover, compared with traditional slow-release fertilizer, biochar had good stability and regeneration performance, alleviating the high cost due to the biochar price. In general, biochar still has potential and prospects as a slow-release material. This study provides support for biochar in mitigating environmental problems associated with excess N.

Keywords: biochar; absorption and desorption performance; optimum biochar use; regeneration; slow-release material



Citation: He, Z.; Wang, C.; Cao, H.; Liang, J.; Pei, S.; Li, Z. Nitrate Absorption and Desorption by Biochar. *Agronomy* **2023**, *13*, 2440. <https://doi.org/10.3390/agronomy13092440>

Academic Editor: Claudio Ciavatta

Received: 3 August 2023

Revised: 15 September 2023

Accepted: 20 September 2023

Published: 21 September 2023



Copyright: © 2023 by the authors. Licensee MDPI, Basel, Switzerland. This article is an open access article distributed under the terms and conditions of the Creative Commons Attribution (CC BY) license (<https://creativecommons.org/licenses/by/4.0/>).

1. Introduction

N fertilizer serves as the primary source of nourishment for approximately 48% of the global population [1], and the demand for maximizing land productivity has led to a further increase in N fertilizer. According to the National Bureau of Statistics of China, the amount of N fertilizer used in China has increased from 9.3 million t in 1980 to 18.3 million t in 2021. The high input of N fertilizer and unequal N balance lead to N leaching [2], weakening the ability of soil to provide nutrients for plant growth and increasing the N content in the receiving water environments [3]. These contribute to reducing N fertilizer utilization efficiency, groundwater pollution, and eutrophication of lake water bodies [1,4,5].

The inorganic N in the soil mainly exists as ammonium (NH_4^+) and nitrate (NO_3^-), with soil colloids having a stronger affinity for NH_4^+ [6]. In comparison, the lower soil anion exchange capacity (AEC) and anion competition (phosphate and sulfate anions) inhibit NO_3^- binding [7,8]. Consequently, soil N leaching is largely dominated by the level of NO_3^- -N [9,10]. To mitigate the adverse environmental impact of NO_3^- -N leaching, NO_3^- -N immobilization is considered a viable method [11,12], and the use of absorbents to bind NO_3^- holds promise for achieving this goal [13]. However, most absorbents are more suitable for the removal of NO_3^- -containing wastewater than for application in soil [3,14,15]. Additionally, the implementation of slow-release fertilizers represents

a useful intervention to reduce NO_3^- -N leaching by releasing nutrients in a controlled manner [16]. Overall, seeking NO_3^- -N absorbents and slow-release materials suitable for soil is a hopeful method to reduce N leaching.

Recently, the utilization of modern waste technology has drawn attention to the preparation of biochar from agricultural waste as an absorbent [17–19]. Biochar, a solid product synthesized using pyrolysis and carbonization in an anaerobic environment [20], exhibits rich pores, a large specific surface area, abundant functional groups, and exchangeable cations, all of which contribute significantly to its excellent absorption capacity [21–23]. Previous studies have proposed biochar as an effective absorbent for NO_3^- -immobilization [24]. Kameyama et al. [25] reported that bagasse biochar absorbs NO_3^- through interaction with functional groups. It is also found that the NO_3^- absorption capacity of modified bagasse biochar is as high as $28.21 \text{ mg}\cdot\text{g}^{-1}$ due to the carbon skeleton and honeycomb structure [26]. Additionally, biochar derived from rice husk can absorb NO_3^- at $2.1 \text{ mg}\cdot\text{g}^{-1}$ [27], and this property has enabled its successful application in reducing NO_3^- leaching from soil [28]. However, not all biochar can be used for NO_3^- absorption [29,30]. This may be related to the raw material and pyrolysis temperature. In other words, the NO_3^- absorption characteristics of biochar need to be carefully verified before using it to reduce N leaching. Furthermore, biochar shows promise as a slow-release fertilizer material [16,31,32] owing to its high aromatic stability and porous structure [33,34]. Lateef et al. [35] reported that biochar derived from corn cob prolongs the nutrient release period. Biochar-based fertilizers are steadier and more consistent than mineral fertilizers, thus reducing the N losses [34]. Compared with pure urea, molten urea-impregnated biochar also has slow-release performance and reduces the N release rate [36]. Similar results were observed after biochar was mixed with urea and minerals [37]. However, despite biochar's potential in absorption and slow-release performance for N, practical application of its sorption and desorption properties remains challenging and faces certain limitations, necessitating further research [16].

The favorable effects of biochar on soil fertility, crop yield, and N loss are closely related to the biochar application rate [1,25,38]. However, there is ongoing debate about the optimal biochar application amount, and no consensus has been reached on the recommended biochar application rate. The range of biochar application varies widely in agricultural production systems, from 1 to $200 \text{ t}\cdot\text{ha}^{-1}$ [39], while from an agronomic and economic standpoint, the appropriate amount is suggested to be $15 \text{ t}\cdot\text{ha}^{-1}$ [40]. Considering the effects of biochar on photosynthesis, an appropriate biochar application rate is suggested to be within the range of $10.1\text{--}20 \text{ t}\cdot\text{ha}^{-1}$ or $2.01\text{--}4\%$ [41]. These may be partly due to differences in biochar performance, N fertilizer application rate, and crop species. For a given biochar, the optimal biochar application rate may depend more on the fertilization regime and soil nutrients [28,32]. Therefore, it is more theoretically significant to determine the optimal biochar application amount based on the biochar absorption and desorption behavior at different nutrient levels.

Under the support of multitudinous advantages of biochar made from different feedstocks [1,28,42,43], high cost is the main factor limiting the large-scale application of biochar. It is reported that the biochar price varies between $\$80 \text{ t}^{-1}$ and $\$13,480 \text{ t}^{-1}$. Despite substantial reductions in production costs owing to technological advancements [44], as an independent farming input, biochar still proves uneconomical [45]. Several investigations have shown that biochar has excellent stability and reusability performance, offering a potential solution to mitigate its high cost [40,46]. Li et al. [47] reported that the lignin-based biochar exhibited excellent reusability. Due to the reversible ion exchange, the absorption efficiency of TI by biochar is as high as 95% after five absorption/desorption cycles [48]. Even after 12 months of biochar application, soil still had high NO_3^- -N content and showed positive effects on crop growth and yield during the second and third year [40]. These imply that biochar has a long-term absorption effect. However, there are few studies on the long-term effects and stability of biochar on NO_3^- -N absorption, which necessitates further exploration.

According to these, compared with previous studies, this study was designed to investigate the absorption and desorption characteristics of NO_3^- -N onto biochar and address the key gaps in the current knowledge by optimizing the biochar dosage and NO_3^- -N concentration to improve the application effectiveness. In addition, by evaluating the regeneration ability, the potential benefits of biochar for nutrient management were explored, providing theoretical support for the long-term economic feasibility of sustainable slow-release fertilizer carriers. The specific objectives are as follows: (i) explore the absorption and desorption behavior of NO_3^- -N onto biochar; (ii) optimize the application rate based on absorption and desorption performance, and (iii) evaluate the recyclability of biochar and its possibility as NO_3^- -N slow-release fertilizer carrier. In summary, this study provides valuable insights into the practical application of biochar in commercial fertilizer product development.

2. Material and Methods

2.1. Soil Preparation and Biochar Production

The soil used in the experiment was taken from a maize field near the Northwest Agriculture and Forestry University ($34^\circ 15' \text{ N}$, $108^\circ 01' \text{ E}$) and consisted of 27.8% clay, 37.7% silt, and 34.5% sand, with a bulk density of $1.35 \text{ g}\cdot\text{cm}^{-3}$. The soil was taken from 0–20 cm of the tillage layer and rinsed with plenty of deionized water, air dried, and sieved through a 2 mm sieve. After air drying, the soil was found to contain $2.3 \text{ mg}\cdot\text{kg}^{-1}$ of NO_3^- -N and $1.9 \text{ mg}\cdot\text{kg}^{-1}$ of NH_4^+ -N.

The biochar was purchased from Shaanxi Yixin Bioenergy Technology Development Co., LTD. The feedstock was apple tree branch pyrolyzed at 450° C for 30 min in the short supply of oxygen. The prepared biochar was manually ground into powder, cleaned with deionized water, and air-dried [49–51]. The soil and biochar were accurately weighed using an electronic weigher (one ten-thousandth). A blender was used to thoroughly mix the soil with the biochar.

2.2. Characterization of the Biochar

The physical and chemical properties of the biochar are shown in Table 1. The pH of the biochar was determined using a pH meter in a 1:5 ratio of biochar to deionized water. The element contents were measured using an elemental analyzer (Elementar Analysensysteme GmbH, Berlin, Germany) coupled with an energy-dispersive X-ray spectroscopy (EDS, Oxford Instruments, Concord, MA, USA). Cation exchange capacity (CEC) is measured using the barium chloride-sulfate forced exchange method [52]. Fourier Transform infrared spectroscopy (FTIR) was obtained using KBr pellets and the Nicolet iS50 FT-IR (Thermo Fisher Scientific Co., Ltd., Waltham, MA, USA) with 16 scans over $400\text{--}4000 \text{ cm}^{-1}$ at a resolution of 2 cm^{-1} to identify the functional groups present on the biochar surface [53,54]. The specific surface area and mean pore diameter of biochar were determined using nitrogen (N_2) sorption–desorption isotherms at -77 K (Belsorp max II instrument, Osaka, Japan). The apparent point of zero charge (pH_{pzc}) was determined using Zetasizer Nano ZS90 (Malvern Instruments, Worcestershire, UK).

Table 1. Physicochemical properties of biochar.

Feedstock	Apple Branch	
pH _{pzc}	3.4	
pH	9.03	
Mean pore size (nm)	5	
Surface area (m ² ·g ⁻¹)	192	
CEC (mol·kg ⁻¹)	50.11	
Element content (%)	C	79.22
	H	2.21
	O	14.01
	N	1.03
	Mg	0.97
	Ca	0.83
	K	0.81

2.3. Absorption Experiment on Biochar

The biochar absorption experiment included two parts: absorption isotherm and kinetic experiments. Various NO₃⁻-N standard solutions were prepared using KNO₃. In the absorption isotherm experiment, 1 g of biochar was placed in a 250 mL conical flask and mixed with a 50 mL solution containing varying initial concentrations of NO₃⁻-N (20–180 mg·L⁻¹). Due to the biochar pH being 9.03, the initial pH of the mixed solution was 8.8 to 9.0. To mitigate the effect of pH on the absorption process, the solution pH was adjusted to 7.0 using 1 mol·L⁻¹ HCl [55]. Use 0.01 mol·L⁻¹ KCl as the background electrolyte [56]. To prevent evaporation of water, the conical flasks were sealed with plastic wrap and stirred at 120 rpm for 4 h at 25 °C. After the absorption process, the solution pH was 7.1–7.2. The suspension samples were then filtered through a 0.45 µm syringe to prevent the influence of biochar on absorbance. The NO₃⁻-N concentrations of the filtrates were measured using the sulfamic acid UV spectrophotometry method (an error of 2% and a measurement range of 0–4 mg·L⁻¹) [57,58]. The specific measurement process was as follows: (1) Transferred the filtrate to a sealed centrifuge tube to prevent evaporation. (2) Prepared standard NO₃⁻-N solutions (0, 0.25, 0.50, 1.00, 1.50, 2.00, 2.50, 3.00, 3.50, and 4.00 mg·L⁻¹) by dissolving KNO₃. Then, 50 mL of each standard solution was mixed with 1 mL of HCL (1 mol·L⁻¹) and 0.1 mL of sulfamic acid (0.8%). Absorbance was measured at 220 nm and 275 nm, and the calibration curve was generated by plotting the NO₃⁻-N concentration (mg·L⁻¹) against the calculated absorbance values at 220 nm minus twice the absorbance values at 275 nm (220 nm–2 × 275 nm) for a series of standard solutions. (3) Determined the absorbance of the filtrate using the same method and calculated the NO₃⁻-N concentration from the calibration curve. (4) If the obtained NO₃⁻-N concentration was outside the measurement range, the filtrate was diluted and then re-measured to improve the accuracy of the measurement.

Similarly, in the absorption kinetic experiment, 1 g of biochar was mixed with 100 mL of a 100 mg·L⁻¹ NO₃⁻-N solution, and the contact time was varied from 0 to 480 min. The experimental conditions, including the pH, stirring speed, temperature, and NO₃⁻-N measurements, were kept identical to those of the absorption isotherm experiment.

2.4. Absorption, Desorption and Regeneration Experiments on Biochar-Soil Mixture

A few drops of chloroform were added during the biochar-soil mixture absorption and desorption experiments to prevent the influence of microorganisms [59,60]. No denitrification in the biochar-soil mixture systems after the use of chloroform. The absorption experiment for the biochar-soil mixture was conducted at varying biochar application rates (0–8%) and initial NO₃⁻-N concentrations (20–240 mg·L⁻¹). Specifically, 13.5 g of the biochar-soil mixture was placed in a PE pipe with a diameter of 1 cm, which was sealed with 100 mesh nylon at the top and bottom. PE pipe and nylon mesh did not absorb NO₃⁻-N. The sealed PE pipe was then immersed in 250 mL of NO₃⁻-N solution with different

initial concentrations. Moreover, the background electrolyte was 0.01 mol·L⁻¹ KCl, and the solution pH was adjusted to 7.0 with 1 mol·L⁻¹ HCl. After 48 h, the solution had a pH of 7.04–7.2, and the NO₃⁻-N concentration in the solution was measured to calculate the absorption capacity of the mixture, following the procedure described previously.

After the absorption experiment, the spent biochar-soil sample was separated from the solution and dried in a vacuum oven at 30 °C. The dried spent biochar-soil mixture sample was then immersed in 1000 mL of deionized water, and the deionized water was replaced every 24 h by transferring a PE pipe containing the soil-biochar mixture with tweezers. Over a duration of 168 h, the NO₃⁻-N concentration in the filtrate was measured to calculate the desorption capacity and efficiency of the mixture. These procedures constituted the biochar-soil mixture desorption experiment. Moreover, the absorption-desorption experiment of 168 h (4% biochar application rate and 80 mg·L⁻¹ NO₃⁻-N concentration) was repeated seven times as the regeneration experiment.

2.5. Data Analysis

The absorption capacity Q_e (mg·g⁻¹) and the absorption rate (%) were calculated as follows [56]:

$$Q_e = V(C_o - C_e)/M \quad (1)$$

$$\text{absorption rate} = 1 - C_e/C_o \times 100\% \quad (2)$$

where C_o and C_e (mg·L⁻¹) are the initial and equilibrium concentrations of NO₃⁻-N, respectively. V (L) and M (g) are the solution volume and mass of dry biochar, respectively. The meanings of Q_e , C_o , and C_e are the same in the following. Considering the difference in absorption capacity between treatments, the relatively low absorption rate can meet the requirement of experimental accuracy [61–63].

Langmuir (Equation (3)) and Freundlich (Equation (4)) isotherm models were employed to describe absorption isotherms of NO₃⁻-N by biochar.

$$Q_e = (Q_{max}K_L C_e)/(1 + K_L C_e) \quad (3)$$

$$Q_e = K_F C_e^{1/n} \quad (4)$$

where Q_{max} (mg·g⁻¹) is the maximum absorption capacity. K_F and K_L are the Freundlich and Langmuir balance constants, respectively. A dimensionless constant separation factor R_L in Langmuir isotherm models is defined as [64]:

$$R_L = 1/(1 + K_L C_o) \quad (5)$$

The absorption kinetics of NO₃⁻-N onto biochar was investigated using the pseudo-first and second-order kinetic models (Equations (6) and (7)), Elovich model (Equation (8)) and Weber-morris intraparticle diffusion model (Equation (9)).

$$\log(Q_e - Q_t) = \log Q_e - k_1 t/2.303 \quad (6)$$

$$t/Q_t = 1/(k_2 Q_e^2) + t/Q_e \quad (7)$$

$$Q_t = (\ln(ab) + \ln t)/b \quad (8)$$

$$Q_t = k_{pi} t^{1/2} + C_i \quad (9)$$

where k_1 (min⁻¹) and k_2 (mg·(g·min)⁻¹) are the pseudo-first and second-order kinetic model absorption rate constant, respectively. Q_t (mg·g⁻¹) is the absorption capacity at time t , respectively. a (mg·(g·min)⁻¹) is the initial absorption rate, and b (mg·g⁻¹) is the desorption constant. k_{pi} (mg·(g·min^{1/2})⁻¹) and C_i are the intraparticle diffusion rate constant and intercept of stage i , respectively.

The biochar desorption efficiency and capacity were obtained by:

$$D_t = \sum_{24}^t V_t C_t \quad (10)$$

$$\eta_t = (D_t - D_{t-24}) / Q_e \quad (11)$$

where D_t ($\text{mg} \cdot \text{g}^{-1}$) is the cumulation desorption capacity at time t . V_t (L) and C_t ($\text{mg} \cdot \text{L}^{-1}$) are the filtrate volume and NO_3^- -N concentration at time t . η_t (%) is the desorption efficiency at time t .

The sustainable index (SI) and Coefficient of variation (CV) were calculated as follows [65]:

$$SI = (\bar{Y} - \sigma) / Y_{max} \quad (12)$$

$$CV = (\sigma / \bar{Y}) \quad (13)$$

where \bar{Y} is 24 h average desorption efficiency/capacity, and Y_{max} is the maximum desorption efficiency/capacity in 24 h. σ is the standard deviation,

Data analysis and statistical tests were performed using SPSS 17.0 (SPSS Inc., Madison, WI, USA) and MATLAB R2020b software (MathWorks Inc., Natick, MA, USA). Diagrams and graphs were drawn using OriginPro 2016 (OriginLab Corporation, Northampton, MA, USA) software.

3. Results

3.1. Characterization

The FTIR spectra exhibited distinguishable differences between the pre- and post-sorption stages of NO_3^- -N onto apple branch biochar (Figure 1). The band around 3420 cm^{-1} corresponded to the valence vibrations of the -OH bands. The intensity of absorption peak at 1585 cm^{-1} corresponds to -COOH, confirming the existence of chemical interactions of NO_3^- -N with biochar. Moreover, apple branch biochar possessed a specific surface area of $192 \text{ m}^2 \cdot \text{g}^{-1}$ and an average pore size of 5 nm (Table 1), establishing a theoretical foundation for the physisorption of NO_3^- -N by biochar [54,66]. The cations in the biochar also contributed to the absorption of NO_3^- -N. However, it is worth noting that the pH_{pzc} and pH of biochar were measured at 3.4 and 9.03 (Table 1), respectively, which may not be favorable for the absorption process. In general, these varied physicochemical properties provide different performances for the absorption of NO_3^- -N onto biochar.

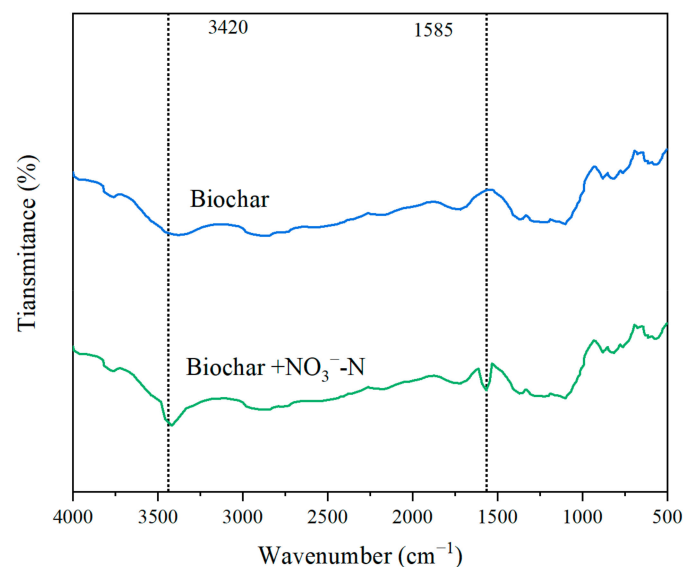


Figure 1. FTIR spectra analysis of pre-sorption and post-sorption biochar samples.

3.2. NO_3^- -N Absorption by Biochar

3.2.1. Absorption Isotherms of NO_3^- -N by Biochar

Figure 2 shows the biochar absorption capacity for NO_3^- -N at different initial NO_3^- -N concentrations. Initial NO_3^- -N concentrations significantly affected the biochar absorption capacity. The absorption capacity first increased with the addition of NO_3^- -N concentration and then gradually stabilized. Obviously, the absorption capacity did not increase linearly with the initial NO_3^- -N concentration. An 800% increase in the initial NO_3^- -N concentration resulted in only a 327% increase in absorption capacity. This is because the high initial NO_3^- -N concentration can enhance the absorption process by overcoming all mass transfer resistances between the liquid and solid phases [67]. However, at elevated NO_3^- -N concentrations, the active biochar sites were the main factor affecting absorption capacity. These findings imply that biochar absorption capacity is governed by both the biochar application amount and NO_3^- -N concentration. Moreover, according to Equation (2), the absorption rate of NO_3^- -N was 39–82% at different initial NO_3^- -N concentrations.

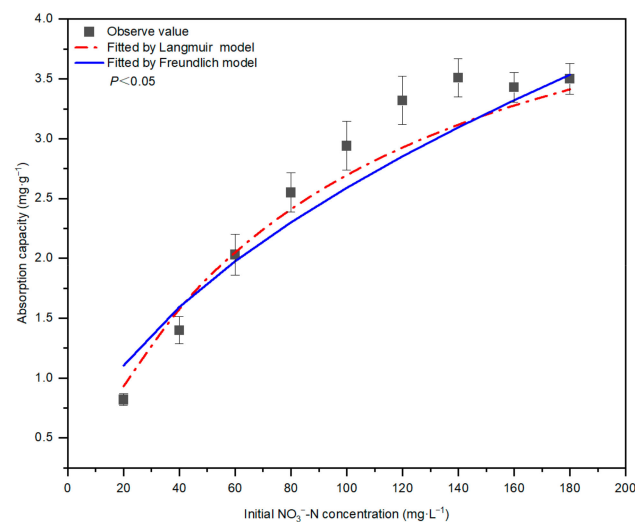


Figure 2. Effect of initial NO_3^- -N concentration on biochar absorption capacity (biochar dosage: 1 g, absorption time: 240 min, temperature: 25 °C).

The absorption isotherm of NO_3^- -N on biochar was simulated using the Freundlich and Langmuir models, and differences in the accuracy of the simulation results were observed in Table 1. The R^2 values for the Langmuir and Freundlich models were 0.977 and 0.946, respectively, indicating a better description of Langmuir model. Moreover, the maximum absorption capacity observed in the Langmuir model was closer to the measured value. However, the value of R^2 for the Freundlich model suggests that the biochar surface is heterogeneous [68]. The high R^2 value of the Langmuir model indicates that biochar absorption sites are energetically identical, and the absorption occurs on a structurally similar binding site [68,69].

The absorption process properties were estimated using equilibrium constants. The value of $1/n$ is a benchmark to assess the adsorbate interaction [70]. In the Freundlich model, the absorption constant $1/n$ was determined to be 0.580 (less than 1), indicating a favorable process [68]. The difficulty of the absorption reaction can be reflected by the value of R_L , calculated using the Langmuir model absorption equilibrium constant K_L (Equation (4)). The value of R_L was in the range of 0.390–0.852, less than 1. It is generally considered that the absorption reaction is easy to proceed. The values of $1/n$ and R_L indicate that the absorption of NO_3^- -N on the biochar surface was favorable.

3.2.2. Absorption Kinetic of NO_3^- -N by Biochar

The effect of contact time on NO_3^- -N uptake by biochar was investigated for a period of 480 min. The absorption capacity of NO_3^- -N by biochar significantly increased with the rising contact time (Figure 3). The biochar absorption capacity was 1.86 and 2.45 $\text{mg}\cdot\text{g}^{-1}$ at the contact time of 5 and 20 min, respectively. As the contact time increased from 20 to 120 min, the biochar absorption capacity accordingly increased from 2.45 to 3.39 $\text{mg}\cdot\text{g}^{-1}$. After 120 min, the absorption capacity was almost constant (increased from 3.39 to 3.51 $\text{mg}\cdot\text{g}^{-1}$), so it can be considered as the equilibrium time. Similarly, the absorption rate of NO_3^- -N showed the same trend, ranging from 68% to 70% after 120 min. From this behavior, it is evident that the absorption process occurred in three steps: the first step was a fast step (0–20 min), followed by a slower second phase (20–120 min), leading to equilibrium.

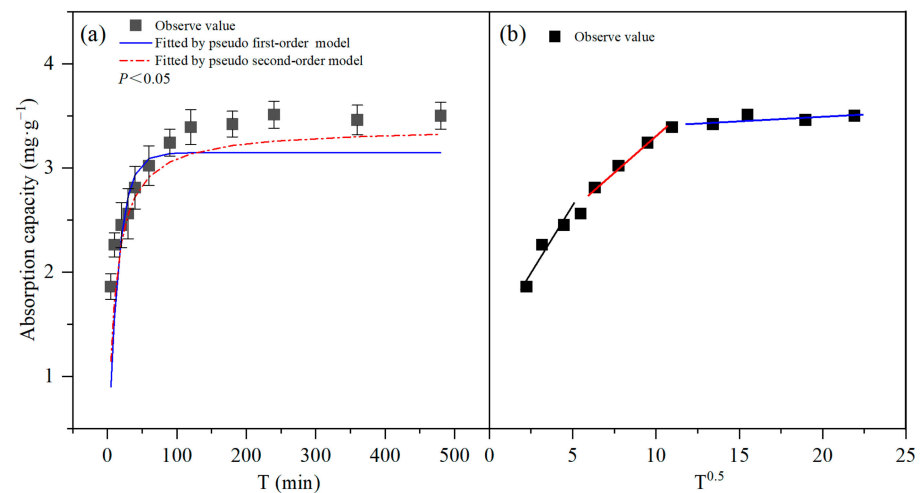


Figure 3. (a) Effect of contact time on biochar absorption capacity; (b) The absorption of NO_3^- -N by fitted with the Weber-morris intraparticle diffusion model (biochar dosage: 1 g, NO_3^- -N concentration: 100 $\text{mg}\cdot\text{L}^{-1}$, temperature: 25 °C). T is the contact time. The different colored lines in (b) represent different diffusion stages.

The Weber-Moriss intraparticle diffusion model was used to distinguish the possible rate control step affecting the absorption kinetics [71]. NO_3^- -N absorption capacity was plotted against $T^{0.5}$ (Figure 3b). Three steps were observed in the pots, and the curve gradually entered a horizontal state from the rising trend at the initial stage. It was also noticed that the diffusion pots did not pass through the origin, which indicated that both film and intraparticle diffusion control and limit the absorption system.

Kinetic models were performed to investigate the mechanism of NO_3^- -N absorption onto biochar. The kinetic absorption data were subjected to the pseudo-first and second-order models, the Elovich model, and the Weber-Moriss intraparticle diffusion model, and model parameters were summarized in Table 2. The R^2 value and calculated Q_e value were used to select the most suitable model for the absorption process. The higher R^2 value suggested that the pseudo-second-order model described the absorption process well as compared to others. Furthermore, the closely calculated Q_e and experimental absorption capacity values provided further support. The R^2 value of 0.947 for the Elovich model proposes a chemisorption process [72].

Table 2. Absorption constants and parameters for the isotherm and kinetic models.

Isotherm models	Langmuir model constants	Q_{max}	6.09
		R_L	0.390–0.852
		R^2	0.977
Freundlich model constants		K	0.189
		$1/n$	0.580
		R^2	0.946
Pseudo-first-order model parameters		Q_e	3.219
		k_1	0.258
		R^2	0.657
Pseudo-second-order model parameters		Q_e	3.449
		k_2	0.048
		R^2	0.903
Elovich model parameter		R^2	0.947
		K_{ip1}	0.256
		R^2	0.912
Weber-Moriss intraparticle diffusion model parameters		K_{ip2}	0.145
		R^2	0.969
		K_{ip3}	0.006
		R^2	0.273

3.3. NO_3^- -N Absorption by Biochar-Soil Mixture

3.3.1. Biochar Application Rate

The NO_3^- -N absorption capacity onto biochar-soil mixture at different biochar application rates is shown in Figure 4. As expected, the application of biochar significantly improved the uptake of NO_3^- -N by soil. At 1% biochar application rate, NO_3^- -N absorption capacity by biochar-soil mixture was about $0.32 \text{ mg}\cdot\text{g}^{-1}$, which was not significantly different from the CK (no added biochar). However, the biochar-soil mixtures had a significantly higher absorption capacity than CK at both the 2% and 4% application rates, with a notable difference between the 2% and 4% application rates. Compared with CK, the absorption capacity increased by 10%, 106%, 162%, and 177% at the biochar application rate of 1%, 2%, 4%, and 8%, respectively. Obviously, the absorption capacity did not proportionally correspond to biochar application rates. Moreover, there was no remarkable difference in absorption capacity between 4% and 8% biochar application rates. This is because when the initial NO_3^- -N concentration is ascertained, a high biochar application rate is prone to competitive absorption, which leads to a decrease in absorption capacity [26]. Absorption rate increased with increasing biochar application rate, with 20%, 22%, 40%, 51%, and 54% for CK, 1%, 2%, 4% and 8% treatment, respectively. Overall, high biochar application rates increased the soil absorption capacity but reduced the biochar application efficiency.

3.3.2. NO_3^- -N Concentration

The effect of NO_3^- -N concentration on biochar-soil mixture absorption capacity was investigated at a 4% biochar application rate with NO_3^- -N concentration ranging from 20 to 240 $\text{mg}\cdot\text{L}^{-1}$ (Figure 5). The response of biochar-soil mixture absorption capacity to NO_3^- -N concentration was consistent with that of biochar. Initial NO_3^- -N concentration greatly affected the absorption capacity. The absorption capacity was 0.284, 0.408, 0.755, 0.801, and $0.837 \text{ mg}\cdot\text{g}^{-1}$ for the NO_3^- -N concentrations of 20, 40, 80, 160, and 240 $\text{mg}\cdot\text{L}^{-1}$, respectively, corresponding to absorption rate of 77%, 55%, 51%, 27%, and 19%. The high absorption capacity occurred for high initial NO_3^- -N concentrations. This increase is due to the fact that higher NO_3^- -N concentration strengthens the driving force between absorbate and improves collision probability between biochar and NO_3^- -N. However, there was no significant difference in the absorption capacity of 80, 160, and 180 $\text{mg}\cdot\text{L}^{-1}$ NO_3^- -N concentrations, which can be explained by the limited number of absorption sites.

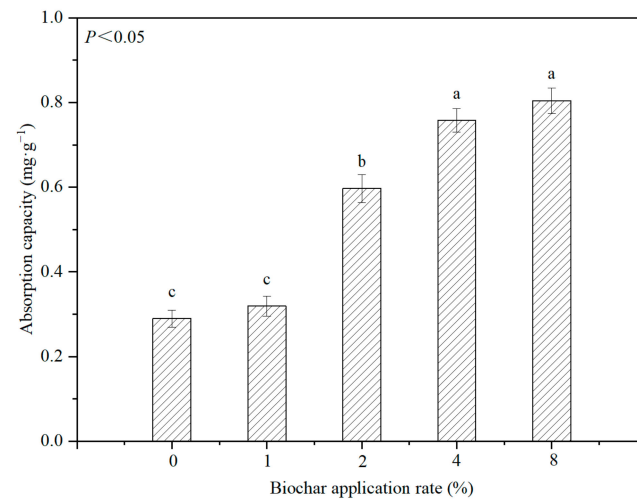


Figure 4. Effect of biochar application rate on absorption capacity (NO_3^- -N concentration: $80 \text{ mg}\cdot\text{L}^{-1}$, absorption time: 48 h, temperature: 25°C). Different letters on the columns represent significant differences between treatments at $p = 0.05$ level.

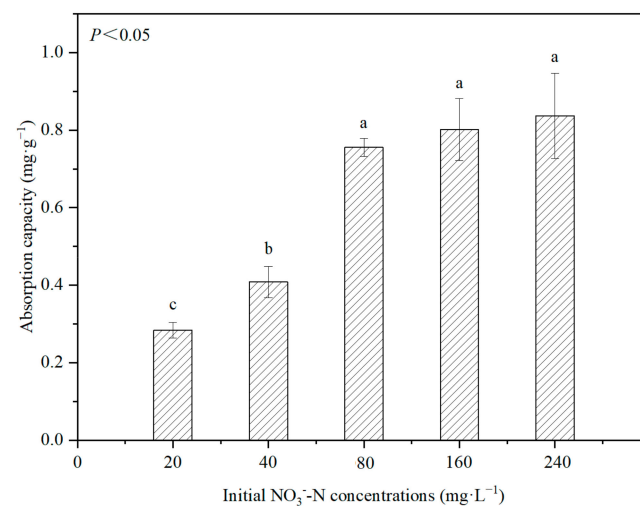


Figure 5. Effect of initial NO_3^- -N concentration on absorption capacity (biochar application rate: 4%, absorption time: 48 h, temperature: 25°C). Different letters on the columns represent significant differences between treatments at $p = 0.05$ level.

3.4. Desorption of NO_3^- -N from Biochar-Soil Mixture

3.4.1. Biochar Application Rate

The desorption efficiency of NO_3^- -N from the soil is significantly affected by biochar addition and desorption time (Figure 6). Regardless of the biochar application rates, the desorption behavior of NO_3^- -N followed a consistent decreasing trend over time. According to the desorption curves, the desorption process exhibited two distinct phases: the initial 24 h and the period after that. Within the first 24 h, all treatments showed the highest NO_3^- -N desorption efficiency, likely due to variations in the binding between NO_3^- -N and biochar, leading to different degrees of adhesion [73]. The most significant difference in desorption efficiency among treatments was also observed during the initial 24 h. Notably, lower biochar application rates resulted in higher desorption efficiency, with the CK treatment showing the highest desorption efficiency. However, beyond the initial 24 h, higher biochar application rates demonstrated a larger desorption efficiency, attributed to varying declining patterns of desorption efficiency. The smooth desorption efficiency curves at high biochar application rates demonstrated that the biochar could obviously

lead to a slower release process of NO_3^- -N in soil, and greater biochar application rates provided better slow-release effects.

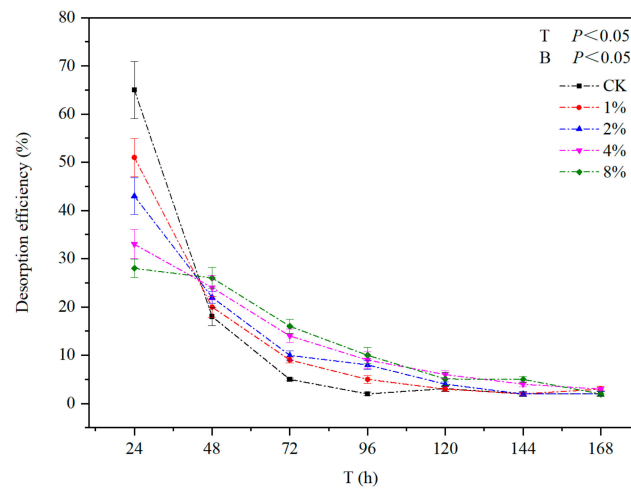


Figure 6. Effect of biochar application rate on desorption efficiency. T and B represent the desorption time and biochar application rate, respectively. (NO_3^- -N concentration: $80 \text{ mg}\cdot\text{L}^{-1}$, temperature: 25°C).

Cumulative desorption capacity is a vital index for evaluating nutrient supply, and it was significantly influenced by the biochar application rate (Figure 7). In the first 24 h, the desorption capacity of NO_3^- -N ranged from 0.164 to $0.256 \text{ mg}\cdot\text{g}^{-1}$ for different biochar application rates. Although the 8% biochar application rate showed the smallest desorption efficiency in the first 24 h (Figure 6), the desorption capacity was still significantly higher than that in CK and the 1% biochar application rate in the first 24 h. This is because the absorption capacity of NO_3^- -N in the 8% biochar application rate was significantly higher than that of CK and 1%. The results also showed that the highest NO_3^- -N desorption capacity was observed at the 2% biochar application rate in the first 24 h, which was attributed to both the high desorption efficiency and NO_3^- -N content in the biochar-soil mixture (Figure 4). This indicates that the desorption capacity of NO_3^- -N in the soil was controlled by the desorption efficiency and absorption capacity, both closely related to the biochar application rate.

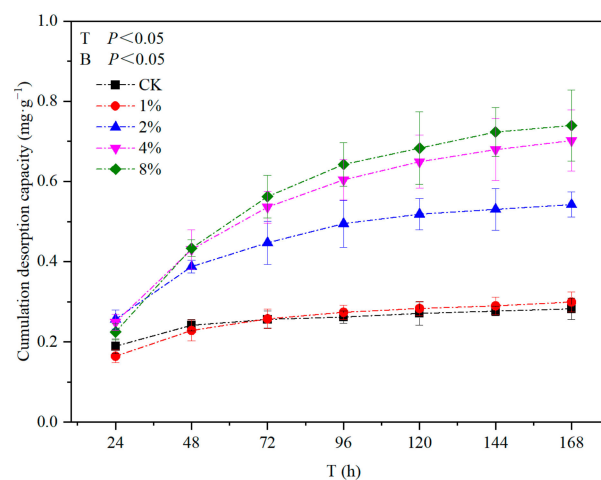


Figure 7. Effect of biochar application rate on cumulation desorption capacity. T and B represent the desorption time and biochar application rate, respectively. (NO_3^- -N concentration: $80 \text{ mg}\cdot\text{L}^{-1}$, temperature: 25°C).

The cumulative desorption capacity of NO_3^- -N over 168 h was 0.283, 0.299, 0.542, 0.702, and 0.739 $\text{mg}\cdot\text{g}^{-1}$ at CK, 1%, 2%, 4%, and 8% biochar application rate, respectively. The cumulative desorption capacity of 2%, 4%, and 8% biochar application rates were significantly higher than 1% and CK. However, there was no significant difference between 1% and CK. Similarly, no significant difference was observed between 4% and 8% biochar application rates. This result could be attributed to insignificant differences in their cumulative desorption efficiency and absorption capacity. Overall, soil with higher biochar application rates exhibited better NO_3^- -N availability, but the cumulative desorption capacity did not consistently increase significantly with biochar addition.

3.4.2. NO_3^- -N Concentration

The desorption behavior at different initial NO_3^- -N concentrations was also investigated (Figure 8). The initial NO_3^- -N concentration had a significant impact on the desorption efficiency and capacity. Similar to different biochar application rates, cumulative desorption capacity increased significantly with increasing NO_3^- -N concentrations. The high NO_3^- -N concentrations could provide more NO_3^- -N (Figure 8). The cumulative desorption capacity of 80, 160, and 240 $\text{mg}\cdot\text{L}^{-1}$ NO_3^- -N concentrations was significantly higher than 20 and 40 $\text{mg}\cdot\text{L}^{-1}$. However, the steeper desorption efficiency curve was observed for the high NO_3^- -N concentration treatment, indicating a poorer slow-release effect. In general, high NO_3^- -N concentrations had better NO_3^- -N supply capacity, while low NO_3^- -N concentrations favored the slow release of NO_3^- -N.

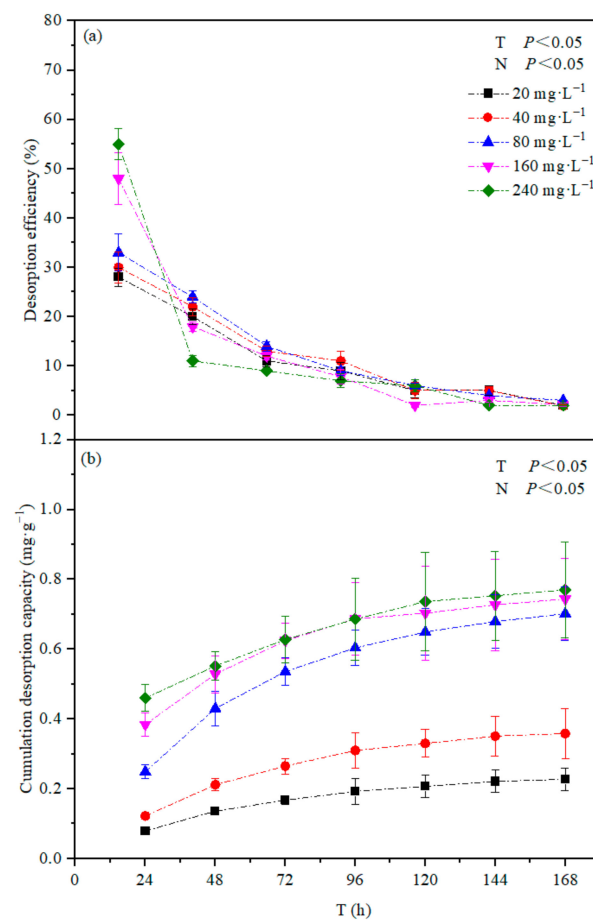


Figure 8. Effect of initial NO_3^- -N concentration on (a) desorption efficiency and (b) cumulation desorption capacity. T and N represent the desorption time and initial NO_3^- -N concentration, respectively. ((a) NO_3^- -N concentration: 80 $\text{mg}\cdot\text{L}^{-1}$, temperature: 25 °C; (b) biochar application rate: 4%, temperature: 25 °C).

3.4.3. Stability and Sustainability of the Desorption Process

The CV and SI were employed to assess the stability and sustainability of the NO_3^- -N desorption process. As shown in Figure 9, both biochar application rate and NO_3^- -N concentration significantly affected the stability and sustainability of desorption efficiency. At different biochar application rates, the maximum (1.68) and minimum (0.80) CV were observed in the CK and 8% biochar application rates, respectively. The lowest and highest CV at different NO_3^- -N concentrations were observed in the 20 and 240 $\text{mg}\cdot\text{L}^{-1}$ NO_3^- -N concentration treatments, respectively. With increasing biochar application rate and NO_3^- -N concentration, the corresponding CV values decreased and increased, respectively, indicating that the high biochar application rate and low NO_3^- -N concentration enhanced the desorption stability. Similar to CV, the high biochar application rate and low NO_3^- -N concentration were conducive to the sustainability of NO_3^- -N desorption due to the higher SI values. This reiterates that the slow-release effect is enhanced by the high biochar application rate and low NO_3^- -N concentration.

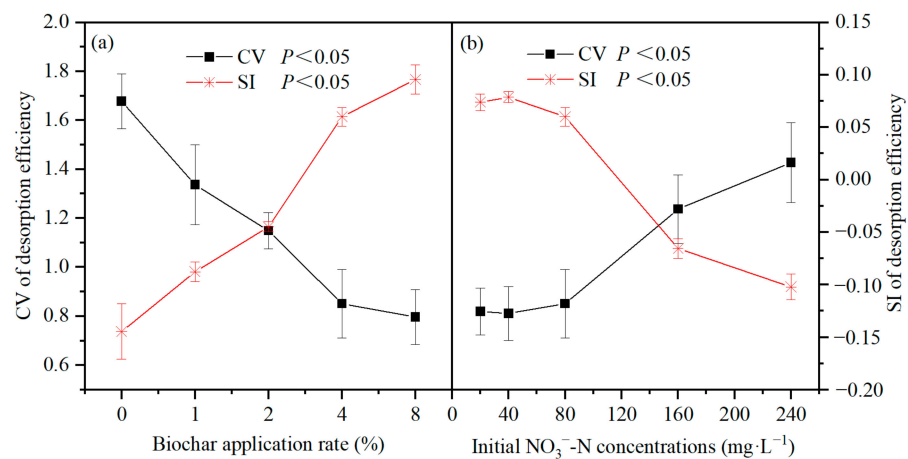


Figure 9. Effect of initial NO_3^- -N concentration and biochar application rate on the stability and sustainability of desorption efficiency ((a) NO_3^- -N concentration: 80 $\text{mg}\cdot\text{L}^{-1}$, desorption time: 168 h, temperature: 25 °C; (b) biochar application rate: 4%, desorption time: 168 h, temperature: 25 °C).

3.5. Optimization of Biochar Application Rate and NO_3^- -N Concentration Management

The cumulative desorption efficiency did not differ significantly between treatments, suggesting that desorption capacity is closely related to absorption capacity. Therefore, the absorption capacity can be used to assess both the absorption and desorption capacity. The difference in desorption efficiency reached its peak in the first 24 h and can represent the slow-release effects of NO_3^- -N. According to the above results, although increasing the biochar application rate and NO_3^- -N concentration can improve the soil absorption capacity, a mismatched combination of biochar application rate and NO_3^- -N concentration does not consistently deliver satisfactory results. For instance, a high biochar application rate with deficient NO_3^- -N generated low absorption capacity (8% biochar application rate with a NO_3^- -N concentration of 80 $\text{mg}\cdot\text{L}^{-1}$ had a lower absorption capacity than 4% biochar application rate with a NO_3^- -N concentration of 240 $\text{mg}\cdot\text{L}^{-1}$; Figures 4 and 5). Similarly, for a given NO_3^- -N supply, the absorption capacity varied considerably (a biochar supply of around 4%, absorption capacity ranged from 0.284 to 0.837 $\text{mg}\cdot\text{g}^{-1}$ in Figure 4), depending on the biochar application rate. This confirms that the absorption capacity would be efficiently amplified at the appropriate biochar application rate and NO_3^- -N concentration. More importantly, high NO_3^- -N concentration significantly increased the desorption efficiency in the first 24 h, which conflicted with the goal of a slow-release effect. Therefore, it is necessary to optimize the management of biochar and NO_3^- -N to maximize the input efficiency while satisfying both the absorption capacity and the slow-release effect.

The response function (the biochar application rate and initial concentration of NO_3^- -N as independent variables and the absorption capacity/desorption efficiency in the first 24 h as response variables) was employed to optimize the biochar application rate and initial NO_3^- -N concentration (Table 3). The coupling effects of biochar application rate and NO_3^- -N concentration on absorption capacity exhibited a downward convex shape (Figure 10a). The maximum absorption capacity ($0.974 \text{ mg}\cdot\text{g}^{-1}$) was achieved when 8.19% of biochar and $219 \text{ mg}\cdot\text{L}^{-1}$ NO_3^- -N concentration was applied. However, the increasing biochar application rate and decreasing NO_3^- -N concentration caused a continuous decrease in desorption efficiency in the first 24 h. The biochar application rate and NO_3^- -N concentration corresponding to the theoretical minimum of desorption efficiency in the first 24 h were not practically significant (Figure 10b). To satisfy both the absorption capacity and the slow-release effect, 80% of the maximum absorption capacity ($0.779 \text{ mg}\cdot\text{g}^{-1}$) and 120% of the measured minimum desorption efficiency in the first 24 h (30%) as the boundary conditions to define the optimal biochar and NO_3^- -N management. The results showed that the absorption capacity of 3.5–12.5% biochar application rate was $0.779 \text{ mg}\cdot\text{g}^{-1}$ at NO_3^- -N concentration ranging from 100 to $330 \text{ mg}\cdot\text{L}^{-1}$. Converting NO_3^- -N concentration to weight, the optimal ratio of biochar to NO_3^- -N varied from 9 to $42.75 \text{ g}\cdot\text{g}^{-1}$. Similarly, the calculation results for the desorption efficiency in the first 24 h were achieved at 1.5–20% biochar application rate with the NO_3^- -N concentration ranging from 10 to $400 \text{ mg}\cdot\text{L}^{-1}$, and the optimal ratio of biochar to NO_3^- -N varied from 27 to $1080 \text{ g}\cdot\text{g}^{-1}$. With careful consideration of various results, when the ratio of biochar to NO_3^- -N was 34– $42.75 \text{ g}\cdot\text{g}^{-1}$, the maximum input efficiency, better nutrient supply, and slow-release effects can be obtained.

Table 3. Regression relationships of biochar application rate and NO_3^- -N concentration with absorption capacity and desorption efficiency in the first 24 h.

Response Variable	Regression Equation	R^2
Absorption capacity (Z_1)	$Z_1 = -0.0189734 + 0.113089x - 0.00948437x^2 + 0.00483395y + 0.00019284xy - 0.0000146292y^2$	0.9194
Desorption efficiency in the first 24 h (Z_2)	$Z_2 = 46.54 - 7.709x + 0.1883y - 0.005531xy + 0.5297x^2 - 0.0002832y^2$	0.9427

Note: x and y represent the biochar application rate (%) and initial NO_3^- -N concentration ($\text{mg}\cdot\text{L}^{-1}$), respectively.

3.6. Regeneration

To investigate the reusability of biochar-soil mixture for NO_3^- -N, the absorption and desorption behaviors were examined for seven consecutive cycles. The repetition cycle significantly affected the absorption capacity and desorption efficiency in the first 24 h (Figure 11). As the repetition cycle increased, the absorption capacity showed a downward trend, mainly due to the incomplete desorption sites. The decreasing rate gradually lessened with each repetition cycle, and stability in the absorption capacity was achieved after five cycles of NO_3^- -N absorption and desorption. Compared with the first cycle, the absorption capacity of NO_3^- -N dropped by about 18% in the seventh cycle. However, the desorption efficiency in the first 24 h was increased significantly with the rise of the repetition cycle. In the first, second, third, fourth, and fifth repetition cycles, the desorption efficiency in the first 24 h was 33%, 39.3%, 41%, 42.9%, and 43.3%, respectively. Similar to the absorption capacity, the desorption efficiency in the first 24 h essentially remained stable after the fifth cycle, ranging from 43% to 44%. Compared with the first cycle, the desorption efficiency in the first 24 h increased by about 10% in the seventh cycle. Generally, the absorption and desorption performance demonstrated that part of the absorption process was irreversible. After the fifth cycle, only reversible absorption was repeated in the NO_3^- -N absorption and desorption process, and the absorption capacity and slow-released effect were not greatly reduced in the subsequent repetition cycles. These

indicate that the reversible absorption is relatively stable, and biochar has excellent cycling properties for the NO_3^- -N absorption.

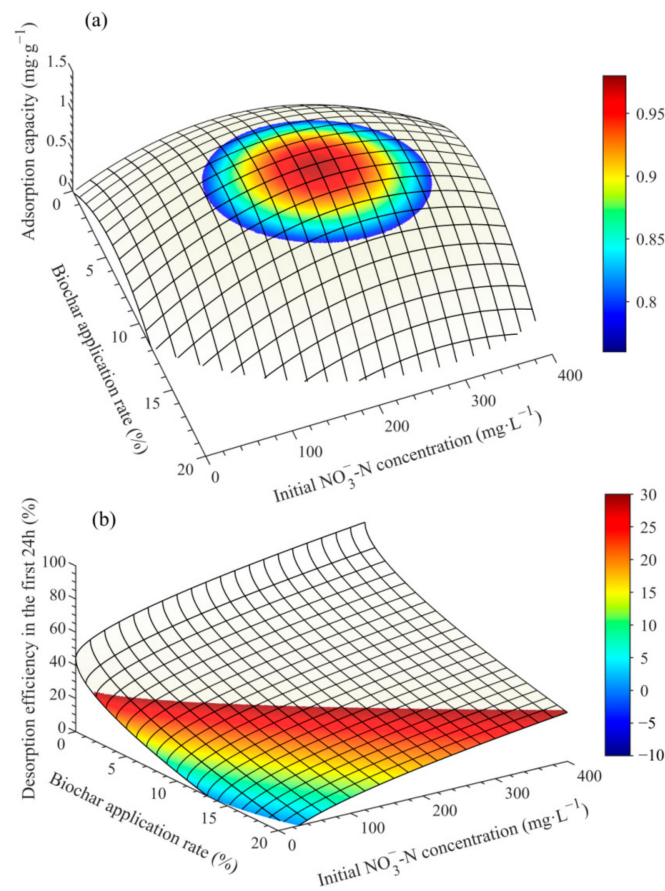


Figure 10. Relationships between absorption capacity, desorption efficiency in the first 24 h and biochar application rate, NO_3^- -N concentration (absorption time 48 h, desorption time: 168 h, temperature: 25 °C). Note: The rainbow-colored area represents the 95% confidence interval for the (a) maximum absorption capacity and (b) minimum desorption efficiency in the first 24 h.

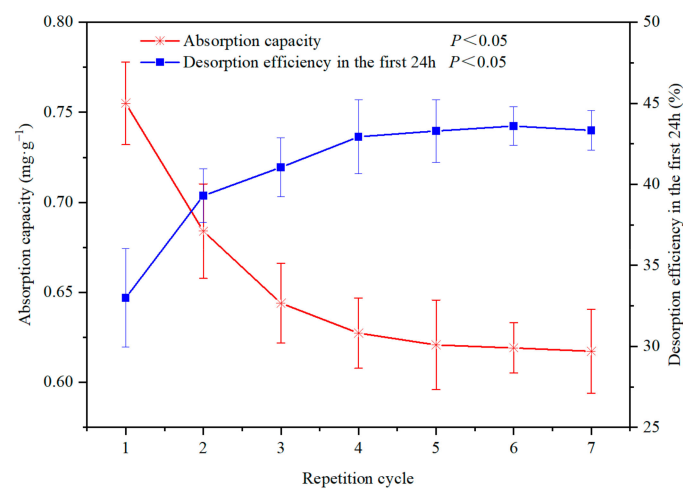


Figure 11. Effect of repetition cycle on biochar absorption capacity and the desorption in the first 24 h (NO_3^- -N concentration: 80 $\text{mg}\cdot\text{L}^{-1}$, biochar application rate: 4%, absorption time: 48 h, desorption time: 24 h, temperature: 25 °C).

4. Discussion

Numerous studies have explored the absorption and desorption of NO_3^- -N by biochar [74], and the absorption capacity of NO_3^- -N onto biochar varies greatly. Due to the net negative surface charge and insufficient AEC, some biochar has almost no NO_3^- -N absorption capacity [29,75]. However, other research findings show contrasting results. For instance, Wang et al. [76] reported that the oak sawdust biochar had an absorption capacity of $2.8 \text{ mg}\cdot\text{g}^{-1}$ for NO_3^- -N and can reduce NO_3^- -N leaching in soil [27]. Similarly, Han et al. [65] also claimed that the absorption capacity of date palm biochar for NO_3^- -N ranged from 0.12 to $7.73 \text{ mg}\cdot\text{g}^{-1}$. In our research, the absorption capacity of NO_3^- -N onto biochar was $3.51 \text{ mg}\cdot\text{g}^{-1}$. This may be due to a considerable specific surface area of the biochar used in our study and an average pore size of 5 nm, exceeding the Stokes ionic radius (0.129 nm) of nitrate and the hydration ionic radius (0.335 nm) [66], suggesting that NO_3^- -N can penetrate into biochar pores [54]. In addition, the presence of metal ions in the biochar provided a positively charged absorption site, contributing to the absorption of NO_3^- -N by electrostatic interaction [54,77]. However, according to Langmuir, the maximum absorption capacity of $6.09 \text{ mg}\cdot\text{g}^{-1}$ for biochar in this study was not very impressive compared to some studies. Biochar made from palm leaf residues had a maximum NO_3^- -N absorption capacity of $42.55 \text{ mg}\cdot\text{g}^{-1}$ [54]. Alsewaileh et al. [70] showed that biochar made from date palm had a maximum NO_3^- -N absorption capacity of $8.37 \text{ mg}\cdot\text{g}^{-1}$. In contrast, the maximum NO_3^- -N absorption capacity of biochar made from mustard straw and wheat straw was $1.3 \text{ mg}\cdot\text{g}^{-1}$ and $1.1 \text{ mg}\cdot\text{g}^{-1}$, respectively. Variations in maximum absorption capacity can be attributed to the diverse physicochemical properties arising from distinct raw materials and production temperatures [43,74,78]. In this study, the small maximum absorption capacity might be attributed to biochar's alkaline pH and pH_{zpc} of 3.4 [54]. Generally, when the solution pH was lower than pH_{zpc} , the surface of the adsorbent was protonated and more positively charged [79,80], which was more favorable for the absorption. However, in this study, the solution pH was higher than the pH_{zpc} , and the electrostatic repulsion between the negatively charged surface sites and NO_3^- -N resulted in lower absorption [81]. In addition, the absorption capacity was also affected by absorption conditions. The absorption capacity was increased with the increasing contact time and initial NO_3^- -N concentration (Figures 2 and 3), which might relate to different mechanisms and limiting factors.

According to the R^2 and the calculated Q_e value from the pseudo-first and second-order models, both physical and chemical absorption were the mechanisms for NO_3^- -N absorption [82]. Moreover, the intensity of absorption peak at 3420 cm^{-1} and 1585 cm^{-1} indicating that biochar formed hydrogen bonds or exchanged ions with NO_3^- -N [81]. The absorption of NO_3^- -N onto biochar involved three consecutive processes [83,84]: (i) film diffusion of the NO_3^- -N to the biochar surface, (ii) intra-particle diffusion of NO_3^- -N into biochar, and (iii) diffusion from macro to micropores. The last process was found to be very rapid in comparison to the other two [85]; therefore, the overall rate of the absorption process depended on the film and intra-particle diffusion processes [85]. Additionally, according to the curve of NO_3^- -N absorption capacity plotted against $T^{0.5}$ did not pass through the origin (Figure 3b), both film and intraparticle diffusion control and limit the absorption system [85]. In summary, the mechanisms and controlling factors of NO_3^- -N absorption by biochar include Van der Waals' force, ion exchange, hydrogen-bond interaction, electrostatic interaction, film diffusion, and intraparticle diffusion (Figure 12).

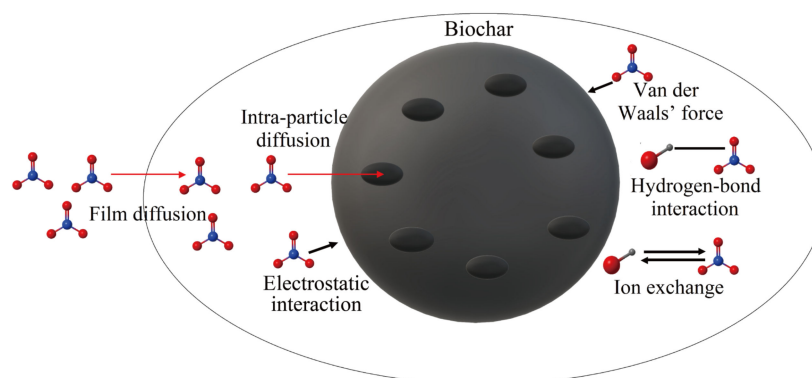


Figure 12. The absorption mechanisms and rate-limiting factors of NO_3^- -N onto biochar.

Due to the ability to absorb NO_3^- -N from solution, placing biochar into soil has also been shown to affect the leaching of NO_3^- -N [24,78,86,87]. In this study, the results showed that biochar increased the soil absorption capacity (Figure 4), which was consistent with previous findings [25]. There might be two reasons for the increased absorption capacity [88]. On the one hand, biochar has a special composition structure, water-ion hydrogen bonding, physical properties, and higher AEC [86,89], which explains a strong absorption capacity for NO_3^- -N [24,90]. In this study, the biochar had 12.1 times the absorption capacity of the soil for NO_3^- -N (Figures 2 and 4). On the other hand, biochar increased the soil porosity and promoted the formation of soil aggregates, thereby improving the ability to absorb and retain NO_3^- -N, resulting in a slow-release desorption process of NO_3^- -N from the soil and biochar mixture [11]. As NO_3^- -N absorption by biochar was controlled by multiple processes [91,92], its desorption process was also expected to be similarly governed [10,93]. Different control mechanisms differed in the intensity of NO_3^- -N absorption, leading to distinct desorption performance. In our study, as reported in earlier studies [94], the rapid desorption efficiency in the first 24 h was observed for NO_3^- -N. This might be related to the weaker bindings and rapid diffusion into the aqueous solutions. Thereafter, the NO_3^- -N desorption was probably governed by the solute diffusion from the porous biochar solid phase into the aqueous phase [95]. This diffusion-limited phase was expected to be slow, probably due to a tortuous porous flow path [94,96].

Notably, similar to pure biochar, the high NO_3^- -N concentration could also increase the biochar-soil mixture absorption capacity (Figure 5). However, the high absorption capacity at a high concentration of NO_3^- -N was not conducive to a slow-release effect. Treatments of 8% biochar application rate with $80 \text{ mg}\cdot\text{L}^{-1}$ NO_3^- -N concentration (Figure 4) had similar NO_3^- -N absorption capacity ($0.8 \text{ mg}\cdot\text{g}^{-1}$) and desorption trends to the 4% biochar application rate with $160 \text{ mg}\cdot\text{L}^{-1}$ NO_3^- -N concentration (Figure 5). However, their desorption efficiency and capacity in the first 24 h were obviously different. The NO_3^- -N desorption efficiency and capacity at 8% biochar application rate with $80 \text{ mg}\cdot\text{L}^{-1}$ NO_3^- -N concentration was 28% and $0.225 \text{ mg}\cdot\text{g}^{-1}$ in the first 24 h, respectively (Figures 6 and 7), while the 4% biochar application rate and $160 \text{ mg}\cdot\text{L}^{-1}$ NO_3^- -N concentration treatment was 48% and $0.384 \text{ mg}\cdot\text{g}^{-1}$, respectively (Figure 8). This result enforced the hypothesis of NO_3^- -N desorption from biochar limiting by multiple processes. The stronger binding sites were occupied first, and the binding strength decreased with the increasing degree of site occupation [43,97]. At higher NO_3^- -N concentrations, the site occupancy was higher, and the absorption strength decreased, which explained the higher NO_3^- -N desorption efficiency at high NO_3^- -N concentrations in the first 24 h. Similarly, it was also observed that the absorption and desorption performance could be controlled by biochar application rate and NO_3^- -N concentration (Figures 4 and 6). Overall, these all affect biochar's effectiveness and ultimately determine the optimal biochar amount.

The optimal biochar application rate was crucial for adopting biochar as a practice due to its availability and price constraints. Existing debates on biochar application rates in agricultural production systems recommended a range from $1 \text{ t}\cdot\text{ha}^{-1}$ to $200 \text{ t}\cdot\text{ha}^{-1}$ [39,98,99].

Positive responses to increasing yields in wheat, maize, rice, and soybeans have been observed for biochar application rates in the range of 1–10 t·ha⁻¹. However, excessive biochar could diminish the positive effects [39]. In the absence of N fertilizer, the application of biochar did not increase the radish yield. However, the radish yield evidently increased with biochar application in the presence of N fertilizer [100]. This implies that the effectiveness of biochar was also related to the amount of fertilizer used. In this study, integrating nutrient supply and slow-release effect, it was recommended to control the application ratio of biochar to NO₃⁻-N at 34–42.75 g·g⁻¹. On this basis, it maximized soil nutrient availability and enhanced the slow-release effect with reduced biochar inputs. Moreover, the perspective of this study was similar to soil testing and fertilizer recommendation; the biochar application rate was only related to the fertilization schedule and soil nutrients. It could greatly accelerate the promotion and application of biochar in different crops and soil conditions.

Due to its excellent absorption and desorption characteristics, biochar was considered a potential sustainable supporting material for the formulation of slow-release fertilizers [42,77]. It has been shown that biochar had a similar nutrient release pattern to Agroblen (conventional slow-release fertilizer) and could improve nutrient loss [92,101,102]. Moreover, biochar impregnated with fertilizer has been used to synthesize or manufacture slow-release fertilizer [37,103–105]. Dominguez et al. [102] reported that the impregnation of N and P fertilizer on oil palm kernel shell biochar improved its nutrient release performance. However, the slow-release effect of biochar-based fertilizer was still facing limitations [16]. Decreased performance in terms of preventing N release was demonstrated by biochar compared to the developed slow-release fertilizers. In this study, NO₃⁻-N desorption efficiency in the first 24 h ranged from 28% to 90% in all treatments, which was higher than the developed formulation [11]. This suggests that although biochar can slow down nutrient desorption efficiency, the unoptimized raw biochar application rate cannot be directly applied to the soil as a slow-release fertilizer material to meet commercial standards [106]. In addition, the absorption capacity of biochar for NO₃⁻-N was 3.51 mg·g⁻¹, lower than that of traditional slow-release fertilizers. In other words, when using biochar as a slow-release fertilizer, a large amount of biochar needed to ensure the growth of plants. Therefore, low N content and high input costs due to low N content need to be focused and solved when developing and applying biochar as slow-release fertilizer.

The nutrient release performance from biochar was related to ion binding capacity and absorption level [16]. Therefore, in addition to optimizing the biochar application rate, biochar modification for absorption capacity and strength has become an inevitable trend to enhance its slow-release effect [107]. Commonly used methods include chemical and physical modifications, with chemical modification being the most extensively employed method. It mainly included acid modification, oxidizing agent modification, carbonaceous materials modification, metal salts, and alkalinity modification. Acid modification could remove impurities such as metals, introduce acid functional groups on the surface, and change the biochar surface area [108]. Modification with oxidizing agents could increase the content of oxygen-containing functional groups on biochar [109]. Biochar modified with montmorillonite had an absorption capacity of up to 9 mg·g⁻¹ [110]. In addition, encapsulation technology combined with nutrient-impregnated biochar has been introduced to improve release performance [111]. Compared to original biochar-based fertilizer, encapsulated biochar-based fertilizer could further improve the slow-release performance [73,94]. Biochar developed by an integrated co-pyrolysis and co-polymerization process could also be used as a potential slow-release fertilizer [112]. These provide new approaches and possibilities for the development and utilization of biochar as a slow-release fertilizer carrier.

Compared with traditional slow-release fertilizers, the high price of biochar is another important factor restricting its application. While biochar has long-term effectiveness compared to traditional slow-release fertilizers, which might reduce its use costs [113]. MnFe-LDO-biochar maintained 80% of antibiotic removal after three consecutive cycles [114]. After seven repeated absorption and desorption of NO₃⁻-N, biochar still showed excel-

lent absorption and slow release of NO_3^- -N (Figure 11). Even as biochar becomes more hydrophilic during aging, aged biochar is expected to absorb more NO_3^- -N compared to fresh biochar [115]. Overall, the long-term effectiveness of biochar might be an important breakthrough in the use of biochar as a slow-release carrier, with both economic and environmental benefits.

Our results highlight the potential benefits of biochar application in improving soil fertility, particularly in the application of slow-release material. However, considering the absence of plant limitations in this study, further field trial studies are needed to systematically understand the long-term interaction between biochar and fertilizer. Of particular interest is the stability and temporal effectiveness of biochar in field environments.

5. Conclusions

In this study, we investigated the kinetics study, isotherms study, and effect of biochar dosage and the NO_3^- -N concentration on the absorption and desorption performance to optimize the biochar application dosage. The biochar from apple branch pyrolysis had an absorption capacity of $3.51 \text{ mg} \cdot \text{g}^{-1}$ for NO_3^- -N. The absorption process could be described by the pseudo-second-order model and Langmuir model. Both biochar application rate and NO_3^- -N concentration influenced the absorption and desorption performance. High biochar rates contributed to a favorable slow-release effect, while low biochar rates contributed to a higher absorption capacity. Satisfactory nutrient supply and slow-release performance were obtained when the ratio of biochar to NO_3^- -N was 34–42.75 $\text{g} \cdot \text{g}^{-1}$. Compared to traditional slow-release fertilizers, biochar was more expensive, had a lower N content of 3.5%, and needed to be applied in large quantities for optimal plant growth, thus requiring significant supplementation costs. Notably, these increased expenses might be mitigated using biochar modification and its sustained effectiveness over time. Overall, combined with optimized biochar absorption and desorption techniques, biochar still has potential and promise as a carrier for slow-release fertilizers in commercial production.

Author Contributions: H.C. and J.L.: Conceived and designed the experiments. Z.H.: Performed the experiments. Analyzed and interpreted the data and results. Wrote the original manuscript. S.P. and C.W.: Performed the experiments. Analyzed and interpreted the data and results. Wrote the original manuscript. J.L.: Analyzed and interpreted the data and results. Z.L.: Provided materials and instrument facilities and monitored the experimental works. J.L. and H.C.: Revised the manuscript and included valuable inputs. All authors have read and agreed to the published version of the manuscript.

Funding: This study was supported by the National Key Research and Development Project (grant number: 2016YFC0400204), the Science and Technology Plan Project of the Water Conservancy Department of Shaanxi Province (grant number: 2020slkj-08), and the National Natural Science Foundation of China (grant number: 52209055).

Data Availability Statement: The data presented in this study are available on request from the corresponding author.

Acknowledgments: We appreciate Bangxin Ding and Qingyang Hu very much for their kind help in conducting the experiment, sampling, and pre-treatment of samples.

Conflicts of Interest: The authors declare no conflict of interest.

References

1. Xia, H.; Riaz, M.; Zhang, M.; Liu, B.; Li, Y.; El-Desouki, Z.; Jiang, C. Biochar-N fertilizer interaction increases N utilization efficiency by modifying soil C/N component under N fertilizer deep placement modes. *Chemosphere* **2022**, *286*, 131594. [[CrossRef](#)] [[PubMed](#)]
2. Tilman, D.; Cassman, K.G.; Matson, P.A.; Naylor, R.; Polasky, S. Agricultural sustainability and intensive production practices. *Nature* **2002**, *418*, 671–677. [[CrossRef](#)] [[PubMed](#)]
3. Heaney, N.; Ukpong, E.; Lin, C. Low-molecular-weight organic acids enable biochar to immobilize nitrate. *Chemosphere* **2020**, *240*, 124872. [[CrossRef](#)] [[PubMed](#)]

4. Beeckman, F.; Motte, H.; Beeckman, T. Nitrification in agricultural soils: Impact, actors and mitigation. *Curr. Opin. Biotechnol.* **2018**, *50*, 166–173. [[CrossRef](#)] [[PubMed](#)]
5. Camargo, J.A.; Alonso, Á. Ecological and toxicological effects of inorganic nitrogen pollution in aquatic ecosystems: A global assessment. *Environ. Int.* **2006**, *32*, 831–849. [[CrossRef](#)] [[PubMed](#)]
6. Dickinson, G.C.; Murphy, K. *Ecosystems: A Functional Approach*; Routledge: London, UK, 1997.
7. Halajnia, A.; Oustan, S.; Najafi, N.; Khataee, A.R.; Lakzian, A. The adsorption characteristics of nitrate on Mg–Fe and Mg–Al layered double hydroxides in a simulated soil solution. *Appl. Clay Sci.* **2012**, *70*, 28–36. [[CrossRef](#)]
8. Li, H.; Chai, L.; Cui, J.; Zhang, F.; Wang, F.; Li, S. Polypyrrole-modified mushroom residue activated carbon for sulfate and nitrate removal from water: Adsorption performance and mechanism. *J. Water Process Eng.* **2022**, *49*, 102916. [[CrossRef](#)]
9. Molenat, J.; Gascuel-Oudou, C.; Ruiz, L.; Gruau, G. Role of water table dynamics on stream nitrate export and concentration in agricultural headwater catchment (France). *J. Hydrol.* **2008**, *348*, 363–378. [[CrossRef](#)]
10. Dupas, R.; Mellander, P.-E.; Gascuel-Oudou, C.; Fovet, O.; McAleer, E.B.; McDonald, N.T.; Shore, M.; Jordan, P. The role of mobilisation and delivery processes on contrasting dissolved nitrogen and phosphorus exports in groundwater fed catchments. *Sci. Total Environ.* **2017**, *599–600*, 1275–1287. [[CrossRef](#)]
11. Gao, Y.; Fang, Z.; Van Zwieten, L.; Bolan, N.; Dong, D.; Quin, B.F.; Meng, J.; Li, F.; Wu, F.; Wang, H.; et al. A critical review of biochar-based nitrogen fertilizers and their effects on crop production and the environment. *Biochar* **2022**, *4*, 36. [[CrossRef](#)]
12. Öztürk, N.; Bektaş, T.E.I. Nitrate removal from aqueous solution by adsorption onto various materials. *J. Hazard. Mater.* **2004**, *112*, 155–162. [[CrossRef](#)] [[PubMed](#)]
13. Bhatnagar, A.; Sillanpää, M. A review of emerging adsorbents for nitrate removal from water. *Chem. Eng. J.* **2011**, *168*, 493–504. [[CrossRef](#)]
14. Çengelöglu, Y.; Kır, E.; Ersöz, M. Removal of fluoride from aqueous solution by using red mud. *Sep. Purif. Technol.* **2002**, *28*, 81–86. [[CrossRef](#)]
15. Mohsenipour, M.; Shahid, S.; Ebrahimi, K. Nitrate Adsorption on Clay Kaolin: Batch Tests. *J. Chem.* **2015**, *2015*, 397069. [[CrossRef](#)]
16. Sim, D.H.H.; Tan, I.A.W.; Lim, L.L.P.; Hameed, B.H. Encapsulated biochar-based sustained release fertilizer for precision agriculture: A review. *J. Clean. Prod.* **2021**, *303*, 127018. [[CrossRef](#)]
17. Liao, X.; Kang, H.; Haidar, G.; Wang, W.; Malghani, S. The impact of biochar on the activities of soil nutrients acquisition enzymes is potentially controlled by the pyrolysis temperature: A meta-analysis. *Geoderma* **2022**, *411*, 115692. [[CrossRef](#)]
18. Gao, S.; DeLuca, T.H. Rangeland application of biochar and rotational grazing interact to influence soil and plant nutrient dynamics. *Geoderma* **2022**, *408*, 115572. [[CrossRef](#)]
19. El-Naggar, A.; Lee, S.S.; Rinklebe, J.; Farooq, M.; Song, H.; Sarmah, A.K.; Zimmerman, A.R.; Ahmad, M.; Shaheen, S.M.; Ok, Y.S. Biochar application to low fertility soils: A review of current status, and future prospects. *Geoderma* **2019**, *337*, 536–554. [[CrossRef](#)]
20. Lehmann, J.; Pereira da Silva, J.; Steiner, C.; Nehls, T.; Zech, W.; Glaser, B. Nutrient availability and leaching in an archaeological Anthrosol and a Ferralsol of the Central Amazon basin: Fertilizer, manure and charcoal amendments. *Plant Soil* **2003**, *249*, 343–357. [[CrossRef](#)]
21. Basso, A.S.; Miguez, F.E.; Laird, D.A.; Horton, R.; Westgate, M. Assessing potential of biochar for increasing water-holding capacity of sandy soils. *GCB Bioenergy* **2013**, *5*, 132–143. [[CrossRef](#)]
22. Lehmann, J.; Rillig, M.C.; Thies, J.; Masiello, C.A.; Hockaday, W.C.; Crowley, D. Biochar effects on soil biota—A review. *Soil Biol. Biochem.* **2011**, *43*, 1812–1836. [[CrossRef](#)]
23. Zhu, H.; Liu, X.; Jiang, Y.; Lin, D.; Yang, K. Sorption kinetics of 1,3,5-trinitrobenzene to biochars produced at various temperatures. *Biochar* **2022**, *4*, 32. [[CrossRef](#)]
24. Singh, B.P.; Hatton, B.J.; Singh, B.; Cowie, A.L.; Kathuria, A. Influence of Biochars on Nitrous Oxide Emission and Nitrogen Leaching from Two Contrasting Soils. *J. Environ. Qual.* **2010**, *39*, 1224–1235. [[CrossRef](#)] [[PubMed](#)]
25. Kameyama, K.; Miyamoto, T.; Shiono, T.; Shinogi, Y. Influence of Sugarcane Bagasse-derived Biochar Application on Nitrate Leaching in Calcaric Dark Red Soil. *J. Environ. Qual.* **2012**, *41*, 1131–1137. [[CrossRef](#)] [[PubMed](#)]
26. Divband Hafshejani, L.; Hooshmand, A.; Naseri, A.A.; Mohammadi, A.S.; Abbasi, F.; Bhatnagar, A. Removal of nitrate from aqueous solution by modified sugarcane bagasse biochar. *Ecol. Eng.* **2016**, *95*, 101–111. [[CrossRef](#)]
27. Pratiwi, E.P.A.; Hillary, A.K.; Fukuda, T.; Shinogi, Y. The effects of rice husk char on ammonium, nitrate and phosphate retention and leaching in loamy soil. *Geoderma* **2016**, *277*, 61–68. [[CrossRef](#)]
28. Jin, Z.; Chen, X.; Chen, C.; Tao, P.; Han, Z.; Zhang, X. Biochar impact on nitrate leaching in upland red soil, China. *Environ. Earth Sci.* **2016**, *75*, 1109. [[CrossRef](#)]
29. Hollister, C.C.; Bisogni, J.J.; Lehmann, J. Ammonium, Nitrate, and Phosphate Sorption to and Solute Leaching from Biochars Prepared from Corn Stover (*Zea mays* L.) and Oak Wood (*Quercus* spp.). *J. Environ. Qual.* **2013**, *42*, 137–144. [[CrossRef](#)]
30. Yang, J.; Li, H.; Zhang, D.; Wu, M.; Pan, B. Limited role of biochars in nitrogen fixation through nitrate adsorption. *Sci. Total Environ.* **2017**, *592*, 758–765. [[CrossRef](#)]
31. An, X.; Wu, Z.; Shi, W.; Qi, H.; Zhang, L.; Xu, X.; Yu, B. Biochar for simultaneously enhancing the slow-release performance of fertilizers and minimizing the pollution of pesticides. *J. Hazard. Mater.* **2021**, *407*, 124865. [[CrossRef](#)]
32. Zhao, L.; Cao, X.; Zheng, W.; Scott, J.; Sharma, B.; Chen, X. Coprolysis of Biomass with Phosphate Fertilizers To Improve Biochar Carbon Retention, Slow Nutrient Release, and Stabilize Heavy Metals in Soil. *ACS Sustain. Chem. Eng.* **2016**, *4*, 1630–1636. [[CrossRef](#)]

33. Dong, D.; Wang, C.; Van Zwieten, L.; Wang, H.; Jiang, P.; Zhou, M.; Wu, W. An effective biochar-based slow-release fertilizer for reducing nitrogen loss in paddy fields. *J Soil Sediments* **2020**, *20*, 3027–3040. [[CrossRef](#)]
34. El Sharkawi, H.M.; Tojo, S.; Chosa, T.; Malhat, F.M.; Youssef, A.M. Biochar-ammonium phosphate as an uncoated-slow release fertilizer in sandy soil. *Biomass Bioenergy* **2018**, *117*, 154–160. [[CrossRef](#)]
35. Lateef, A.; Nazir, R.; Jamil, N.; Alam, S.; Shah, R.; Khan, M.N.; Saleem, M. Synthesis and characterization of zeolite based nano-composite: An environment friendly slow release fertilizer. *Microporous Mesoporous Mater.* **2016**, *232*, 174–183. [[CrossRef](#)]
36. Zhong, X.; Wang, M.; Jiang, E. Preparation of an Environment-friendly Biochar Fertilizer. *IOP Conf. Ser. Mater. Sci. Eng.* **2018**, *301*, 012157. [[CrossRef](#)]
37. Shi, W.; Ju, Y.; Bian, R.; Li, L.; Joseph, S.; Mitchell, D.R.G.; Munroe, P.; Taherymoosavi, S.; Pan, G. Biochar bound urea boosts plant growth and reduces nitrogen leaching. *Sci. Total Environ.* **2020**, *701*, 134424. [[CrossRef](#)] [[PubMed](#)]
38. Cao, D.; Lan, Y.; Chen, W.; Yang, X.; Wang, D.; Ge, S.; Yang, J.; Wang, Q. Successive applications of fertilizers blended with biochar in the soil improve the availability of phosphorus and productivity of maize (*Zea mays* L.). *Eur. J. Agron.* **2021**, *130*, 126344. [[CrossRef](#)]
39. Farhangi-Abriz, S.; Torabian, S.; Qin, R.; Noulas, C.; Lu, Y.; Gao, S. Biochar effects on yield of cereal and legume crops using meta-analysis. *Sci. Total Environ.* **2021**, *775*, 145869. [[CrossRef](#)]
40. Pandit, N.R.; Mulder, J.; Hale, S.E.; Zimmerman, A.R.; Pandit, B.H.; Cornelissen, G. Multi-year double cropping biochar field trials in Nepal: Finding the optimal biochar dose through agronomic trials and cost-benefit analysis. *Sci. Total Environ.* **2018**, *637–638*, 1333–1341. [[CrossRef](#)]
41. Gao, Y.; Shao, G.; Yang, Z.; Zhang, K.; Lu, J.; Wang, Z.; Wu, S.; Xu, D. Influences of soil and biochar properties and amount of biochar and fertilizer on the performance of biochar in improving plant photosynthetic rate: A meta-analysis. *Eur. J. Agron.* **2021**, *130*, 126345. [[CrossRef](#)]
42. Clough, T.J.; Condon, L.M.; Kammann, C.; Müller, C. A Review of Biochar and Soil Nitrogen Dynamics. *Agronomy* **2013**, *3*, 275–293. [[CrossRef](#)]
43. Hale, S.E.; Alling, V.; Martinsen, V.; Mulder, J.; Breedveld, G.D.; Cornelissen, G. The sorption and desorption of phosphate-P, ammonium-N and nitrate-N in cacao shell and corn cob biochars. *Chemosphere* **2013**, *91*, 1612–1619. [[CrossRef](#)] [[PubMed](#)]
44. Vochozka, M.; Maroušková, A.; Váchal, J.; Straková, J. Biochar pricing hampers biochar farming. *Clean Technol. Environ. Policy* **2016**, *18*, 1225–1231. [[CrossRef](#)]
45. Clare, A.; Barnes, A.; McDonagh, J.; Shackley, S. From rhetoric to reality: Farmer perspectives on the economic potential of biochar in China. *Int. J. Agric. Sustain.* **2014**, *12*, 440–458. [[CrossRef](#)]
46. Singh, M.; Ahsan, M.; Pandey, V.; Singh, A.; Mishra, D.; Tiwari, N.; Singh, P.; Karak, T.; Khare, P. Comparative assessment for removal of anionic dye from water by different waste-derived biochar vis a vis reusability of generated sludge. *Biochar* **2022**, *4*, 13. [[CrossRef](#)]
47. Li, Y.; Wang, F.; Miao, Y.; Mai, Y.; Li, H.; Chen, X.; Chen, J. A lignin-biochar with high oxygen-containing groups for adsorbing lead ion prepared by simultaneous oxidization and carbonization. *Bioresour. Technol.* **2020**, *307*, 123165. [[CrossRef](#)] [[PubMed](#)]
48. Li, H.; Xiong, J.; Xiao, T.; Long, J.; Wang, Q.; Li, K.; Liu, X.; Zhang, G.; Zhang, H. Biochar derived from watermelon rinds as regenerable adsorbent for efficient removal of thallium(I) from wastewater. *Process Saf. Environ. Prot.* **2019**, *127*, 257–266. [[CrossRef](#)]
49. Tao, B.; Chen, Q.; Jiang, Y.; Zhang, B.; Yuan, H.; Wang, Y. Effect of particle sizes of biochar on CO₂ emissions in a poplar plantation of ancient Yellow River channel, China. *J. Environ. Manag.* **2023**, *345*, 118721. [[CrossRef](#)]
50. Shi, R.-Y.; Ni, N.; Wang, R.-H.; Nkoh, J.N.; Pan, X.-Y.; Dong, G.; Xu, R.-K.; Cui, X.-M.; Li, J.-Y. Dissolved biochar fractions and solid biochar particles inhibit soil acidification induced by nitrification through different mechanisms. *Sci. Total Environ.* **2023**, *874*, 162464. [[CrossRef](#)]
51. Suresh Kumar, P.; Korving, L.; Keesman, K.J.; van Loosdrecht, M.C.M.; Witkamp, G.-J. Effect of pore size distribution and particle size of porous metal oxides on phosphate adsorption capacity and kinetics. *Chem. Eng. J.* **2019**, *358*, 160–169. [[CrossRef](#)]
52. Wang, T.; Zheng, J.; Liu, H.; Peng, Q.; Zhou, H.; Zhang, X. Adsorption characteristics and mechanisms of Pb²⁺ and Cd²⁺ by a new agricultural waste—*Caragana korshinskii* biomass derived biochar. *Environ. Sci. Pollut. Res.* **2021**, *28*, 13800–13818. [[CrossRef](#)] [[PubMed](#)]
53. Zhang, J.-P.; Zhang, F.-S. Recycling waste polyethylene film for amphoteric superabsorbent resin synthesis. *Chem. Eng. J.* **2018**, *331*, 169–176. [[CrossRef](#)]
54. Wang, T.; Zhang, D.; Fang, K.; Zhu, W.; Peng, Q.; Xie, Z. Enhanced nitrate removal by physical activation and Mg/Al layered double hydroxide modified biochar derived from wood waste: Adsorption characteristics and mechanisms. *J. Environ. Chem. Eng.* **2021**, *9*, 105184. [[CrossRef](#)]
55. Tan, G.; Mao, Y.; Wang, H.; Xu, N. A comparative study of arsenic(V), tetracycline and nitrate ions adsorption onto magnetic biochars and activated carbon. *Chem. Eng. Res. Des.* **2020**, *159*, 582–591. [[CrossRef](#)]
56. Wang, T.; Liu, H.; Duan, C.; Xu, R.; Zhang, Z.; She, D.; Zheng, J. The Eco-Friendly Biochar and Valuable Bio-Oil from *Caragana korshinskii*: Pyrolysis Preparation, Characterization, and Adsorption Applications. *Materials* **2020**, *13*, 3391. [[CrossRef](#)] [[PubMed](#)]
57. Muhammad, I.; Yang, L.; Ahmad, S.; Farooq, S.; Khan, A.; Zeeshan, M.; Zhou, X.B. Low Irrigation Water Improves Biomass Saccharification, Photosynthetic Pigments of Maize, and Minimizes Nitrate Nitrogen Leaching. *J. Soil Sci. Plant Nutr.* **2022**, *22*, 4897–4912. [[CrossRef](#)]

58. Zhang, Z.; Huang, G.; Zhang, P.; Shen, J.; Wang, S.; Li, Y. Development of iron-based biochar for enhancing nitrate adsorption: Effects of specific surface area, electrostatic force, and functional groups. *Sci. Total Environ.* **2023**, *856*, 159037. [[CrossRef](#)] [[PubMed](#)]
59. Lu, S.; Jin, X.; Guo, J.; Sheng, L. Effect of CH₃Cl as inhibitor in sediment-water system on nitrogen transformation. *Ecol. Environ.* **2006**, *15*, 1133–1137.
60. Wang, B.; Zhao, S.; Qin, Z.; Gao, Q.; Lou, Y.; Liu, S. Effect of biochar on adsorption-desorption characteristics of nitrate nitrogen in black soil. *J. Agro-Environ. Sci.* **2016**, *35*, 115–121.
61. Tomczyk, A.; Kondracki, B.; Szewczuk-Karpisz, K. Chemical modification of biochars as a method to improve its surface properties and efficiency in removing xenobiotics from aqueous media. *Chemosphere* **2023**, *312*, 137238. [[CrossRef](#)]
62. Zhou, Y.; Gao, B.; Zimmerman, A.R.; Fang, J.; Sun, Y.; Cao, X. Sorption of heavy metals on chitosan-modified biochars and its biological effects. *Chem. Eng. J.* **2013**, *231*, 512–518. [[CrossRef](#)]
63. Zhang, M.; Gao, B.; Yao, Y.; Xue, Y.; Inyang, M. Synthesis of porous MgO-biochar nanocomposites for removal of phosphate and nitrate from aqueous solutions. *Chem. Eng. J.* **2012**, *210*, 26–32. [[CrossRef](#)]
64. Foo, K.Y.; Hameed, B.H. Insights into the modeling of adsorption isotherm systems. *Chem. Eng. J.* **2010**, *156*, 2–10. [[CrossRef](#)]
65. Han, X.; Hu, C.; Chen, Y.; Qiao, Y.; Liu, D.; Fan, J.; Li, S.; Zhang, Z. Crop yield stability and sustainability in a rice-wheat cropping system based on 34-year field experiment. *Eur. J. Agron.* **2020**, *113*, 125965. [[CrossRef](#)]
66. Sundaram, S.K.; Saraswathi, S.; Jayalakshmi, S.; Lalitha, S. Estimation of solvated ionic radii of bivalent nitrates through molal hydration number. *Bull. Electrochem.* **2003**, *19*, 217–220.
67. Qu, B.; Zhou, J.; Xiang, X.; Zheng, C.; Zhao, H.; Zhou, X. Adsorption behavior of Azo Dye C. I. Acid Red 14 in aqueous solution on surface soils. *J. Environ. Sci.* **2008**, *20*, 704–709. [[CrossRef](#)] [[PubMed](#)]
68. Kizito, S.; Wu, S.; Kipkemoi Kirui, W.; Lei, M.; Lu, Q.; Bah, H.; Dong, R. Evaluation of slow pyrolyzed wood and rice husks biochar for adsorption of ammonium nitrogen from piggery manure anaerobic digestate slurry. *Sci. Total Environ.* **2015**, *505*, 102–112. [[CrossRef](#)]
69. Al-Ghouti, M.A.; Da'ana, D.A. Guidelines for the use and interpretation of adsorption isotherm models: A review. *J. Hazard. Mater.* **2020**, *393*, 122383. [[CrossRef](#)]
70. Santhana Krishna Kumar, A.; Ramachandran, R.; Kalidhasan, S.; Rajesh, V.; Rajesh, N. Potential application of dodecylamine modified sodium montmorillonite as an effective adsorbent for hexavalent chromium. *Chem. Eng. J.* **2012**, *211–212*, 396–405. [[CrossRef](#)]
71. Wu, Z.; Zhong, H.; Yuan, X.; Wang, H.; Wang, L.; Chen, X.; Zeng, G.; Wu, Y. Adsorptive removal of methylene blue by rhamnolipid-functionalized graphene oxide from wastewater. *Water Res.* **2014**, *67*, 330–344. [[CrossRef](#)]
72. Ho, Y.S.; McKay, G. Pseudo-second order model for sorption processes. *Process Biochem.* **1999**, *34*, 451–465. [[CrossRef](#)]
73. Ye, Z.; Zhang, L.; Huang, Q.; Tan, Z. Development of a carbon-based slow release fertilizer treated by bio-oil coating and study on its feedback effect on farmland application. *J. Clean. Prod.* **2019**, *239*, 118085. [[CrossRef](#)]
74. Yin, Q.; Zhang, B.; Wang, R.; Zhao, Z. Biochar as an adsorbent for inorganic nitrogen and phosphorus removal from water: A review. *Environ. Sci. Pollut. Res.* **2017**, *24*, 26297–26309. [[CrossRef](#)] [[PubMed](#)]
75. Yao, Y.; Gao, B.; Zhang, M.; Inyang, M.; Zimmerman, A.R. Effect of biochar amendment on sorption and leaching of nitrate, ammonium, and phosphate in a sandy soil. *Chemosphere* **2012**, *89*, 1467–1471. [[CrossRef](#)] [[PubMed](#)]
76. Wang, Z.; Guo, H.; Shen, F.; Yang, G.; Zhang, Y.; Zeng, Y.; Wang, L.; Xiao, H.; Deng, S. Biochar produced from oak sawdust by Lanthanum (La)-involved pyrolysis for adsorption of ammonium (NH₄⁺), nitrate (NO₃⁻), and phosphate (PO₄³⁻). *Chemosphere* **2015**, *119*, 646–653. [[CrossRef](#)] [[PubMed](#)]
77. González, M.E.; Cea, M.; Medina, J.; González, A.; Díez, M.C.; Cartes, P.; Monreal, C.; Navia, R. Evaluation of biodegradable polymers as encapsulating agents for the development of a urea controlled-release fertilizer using biochar as support material. *Sci. Total Environ.* **2015**, *505*, 446–453. [[CrossRef](#)] [[PubMed](#)]
78. Liu, Y.; Liu, S.; Yang, Z.; Xiao, L. Synergetic effects of biochars and denitrifier on nitrate removal. *Bioresour. Technol.* **2021**, *335*, 125245. [[CrossRef](#)] [[PubMed](#)]
79. Li, W.; Pierre-Louis, A.-M.; Kwon, K.D.; Kubicki, J.D.; Strongin, D.R.; Phillips, B.L. Molecular level investigations of phosphate sorption on corundum (α -Al₂O₃) by ³¹P solid state NMR, ATR-FTIR and quantum chemical calculation. *Geochim. Cosmochim. Acta* **2013**, *107*, 252–266. [[CrossRef](#)]
80. Yang, X.; Wang, D.; Sun, Z.; Tang, H. Adsorption of phosphate at the aluminum (hydr)oxides–water interface: Role of the surface acid–base properties. *Colloids Surf. Physicochem. Eng. Aspects* **2007**, *297*, 84–90. [[CrossRef](#)]
81. Li, R.; Wang, J.J.; Zhou, B.; Zhang, Z.; Liu, S.; Lei, S.; Xiao, R. Simultaneous capture removal of phosphate, ammonium and organic substances by MgO impregnated biochar and its potential use in swine wastewater treatment. *J. Clean. Prod.* **2017**, *147*, 96–107. [[CrossRef](#)]
82. Yin, Q.; Wang, R.; Zhao, Z. Application of Mg–Al-modified biochar for simultaneous removal of ammonium, nitrate, and phosphate from eutrophic water. *J. Clean. Prod.* **2018**, *176*, 230–240. [[CrossRef](#)]
83. Kołodziejka, D.; Wnętrzak, R.; Leahy, J.J.; Hayes, M.H.B.; Kwapiński, W.; Hubicki, Z. Kinetic and adsorptive characterization of biochar in metal ions removal. *Chem. Eng. J.* **2012**, *197*, 295–305. [[CrossRef](#)]
84. Wang, Y.; Srinivasakannan, C.; Wang, H.; Xue, G.; Wang, L.; Wang, X.; Duan, X. Preparation of novel biochar containing graphene from waste bamboo with high methylene blue adsorption capacity. *Diam. Relat. Mater.* **2022**, *125*, 109034. [[CrossRef](#)]

85. Simha, P.; Yadav, A.; Pinjari, D.; Pandit, A.B. On the behaviour, mechanistic modelling and interaction of biochar and crop fertilizers in aqueous solutions. *Resour. Technol.* **2016**, *2*, 133–142. [[CrossRef](#)]
86. Dempster, D.; Jones, D.; Murphy, D. Clay and biochar amendments decreased inorganic but not dissolved organic nitrogen leaching in soil. *Soil Res.* **2012**, *50*, 216. [[CrossRef](#)]
87. Vijayaraghavan, K.; Balasubramanian, R. Application of pinewood waste-derived biochar for the removal of nitrate and phosphate from single and binary solutions. *Chemosphere* **2021**, *278*, 130361. [[CrossRef](#)]
88. Chen, M.; Wang, F.; Zhang, D.-L.; Yi, W.-M. Effect of Biochar Structure on Adsorption Characteristics of Ammonia Nitrogen. *J. Environ. Sci.* **2019**, *40*, 5421–5429.
89. Kammann, C.I.; Schmidt, H.-P.; Messerschmidt, N.; Linsel, S.; Steffens, D.; Müller, C.; Koyro, H.-W.; Conte, P.; Joseph, S. Erratum: Plant growth improvement mediated by nitrate capture in co-composted biochar. *Sci. Rep.* **2015**, *5*, 12378. [[CrossRef](#)]
90. Liang, B.; Lehmann, J.; Solomon, D.; Kinyangi, J.; Grossman, J.; O'Neill, B.; Skjemstad, J.O.; Thies, J.; Luizão, F.J.; Petersen, J.; et al. Black carbon increases cation exchange capacity in soils. *Soil Sci. Soc. Am. J.* **2006**, *70*, 1719–1730. [[CrossRef](#)]
91. Luo, W.; Qian, L.; Liu, W.; Zhang, X.; Wang, Q.; Jiang, H.; Cheng, B.; Ma, H.; Wu, Z. A potential Mg-enriched biochar fertilizer: Excellent slow-release performance and release mechanism of nutrients. *Sci. Total Environ.* **2021**, *768*, 144454. [[CrossRef](#)]
92. Tran, H.N.; You, S.; Hosseini-Bandegharai, A.; Chao, H. Mistakes and inconsistencies regarding adsorption of contaminants from aqueous solutions: A critical review. *Water Res.* **2017**, *120*, 88–116. [[CrossRef](#)] [[PubMed](#)]
93. Liu, X.; Liao, J.; Song, H.; Yang, Y.; Guan, C.; Zhang, Z. A Biochar-Based Route for Environmentally Friendly Controlled Release of Nitrogen: Urea-Loaded Biochar and Bentonite Composite. *Sci. Rep.* **2019**, *9*, 9548. [[CrossRef](#)] [[PubMed](#)]
94. Gwenz, W.; Nyambishi, T.J.; Chaukura, N.; Mapope, N. Synthesis and nutrient release patterns of a biochar-based N-P-K slow-release fertilizer. *Int. J. Environ. Sci. Technol.* **2018**, *15*, 405–414. [[CrossRef](#)]
95. Onishi, B.S.D.; dos Reis Ferreira, C.S.; Urbano, A.; Santos, M.J. Modified hydrotalcite for phosphorus slow-release: Kinetic and sorption-desorption processes in clayey and sandy soils from North of Paraná state (Brazil). *Appl. Clay Sci.* **2020**, *197*, 105759. [[CrossRef](#)]
96. Dünisch, O.; Lima, V.C.; Seehann, G.; Donath, J.; Montóia, V.R.; Schwarz, T. Retention properties of wood residues and their potential for soil amelioration. *Wood Sci. Technol.* **2006**, *41*, 169. [[CrossRef](#)]
97. Srividya, K.; Mohanty, K. Biosorption of hexavalent chromium from aqueous solutions by *Catla catla* scales: Equilibrium and kinetics studies. *Chem. Eng. J.* **2009**, *155*, 666–673. [[CrossRef](#)]
98. Intani, K.; Latif, S.; Islam, M.S.; Müller, J. Phytotoxicity of Corn cob Biochar before and after Heat Treatment and Washing. *Sustainability* **2019**, *11*, 30. [[CrossRef](#)]
99. Van Zwieten, L.; Kimber, S.; Morris, S.; Chan, K.Y.; Downie, A.; Rust, J.; Joseph, S.; Cowie, A. Effects of biochar from slow pyrolysis of papermill waste on agronomic performance and soil fertility. *Plant Soil* **2010**, *327*, 235–246. [[CrossRef](#)]
100. Chan, K.Y.; Van Zwieten, L.; Meszaros, I.; Downie, A.; Joseph, S. Using poultry litter biochars as soil amendments. *Aust. J. Soil Res.* **2008**, *46*, 437–444. [[CrossRef](#)]
101. Chen, Q.; Qin, J.; Sun, P.; Cheng, Z.; Shen, G. Cow dung-derived engineered biochar for reclaiming phosphate from aqueous solution and its validation as slow-release fertilizer in soil-crop system. *J. Clean. Prod.* **2018**, *172*, 2009–2018. [[CrossRef](#)]
102. Dominguez, E.L.; Uttran, A.; Loh, S.K.; Manero, M.-H.; Upperton, R.; Idris Tanimu, M.; Thomas Bachmann, R. Characterisation of industrially produced oil palm kernel shell biochar and its potential as slow release nitrogen-phosphate fertilizer and carbon sink. *Mater. Today Proc.* **2020**, *31*, 221–227. [[CrossRef](#)]
103. Khan, H.A.; Naqvi, S.R.; Mehran, M.T.; Khoja, A.H.; Khan Niazi, M.B.; Juchelková, D.; Atabani, A. A performance evaluation study of nano-biochar as a potential slow-release nano-fertilizer from wheat straw residue for sustainable agriculture. *Chemosphere* **2021**, *285*, 131382. [[CrossRef](#)]
104. Kumar Awasthi, M.; Wang, M.; Pandey, A.; Chen, H.; Kumar Awasthi, S.; Wang, Q.; Ren, X.; Hussain Lahori, A.; Li, D.-S.; Li, R.; et al. Heterogeneity of zeolite combined with biochar properties as a function of sewage sludge composting and production of nutrient-rich compost. *Waste Manag.* **2017**, *68*, 760–773. [[CrossRef](#)] [[PubMed](#)]
105. Wu, Y.; Brickler, C.; Li, S.; Chen, G. Synthesis of microwave-mediated biochar-hydrogel composites for enhanced water absorbency and nitrogen release. *Polym. Test.* **2021**, *93*, 106996. [[CrossRef](#)]
106. Naz, M.Y.; Sulaiman, S.A. Testing of starch-based carbohydrate polymer coatings for enhanced urea performance. *J. Coat. Technol. Res.* **2014**, *11*, 747–756. [[CrossRef](#)]
107. He, Q.; Li, X.; Ren, Y. Analysis of the simultaneous adsorption mechanism of ammonium and phosphate on magnesium-modified biochar and the slow release effect of fertiliser. *Biochar* **2022**, *4*, 25. [[CrossRef](#)]
108. Peng, P.; Lang, Y.-H.; Wang, X.-M. Adsorption behavior and mechanism of pentachlorophenol on reed biochars: pH effect, pyrolysis temperature, hydrochloric acid treatment and isotherms. *Ecol. Eng.* **2016**, *90*, 225–233. [[CrossRef](#)]
109. Xue, Y.; Gao, B.; Yao, Y.; Inyang, M.; Zhang, M.; Zimmerman, A.R.; Ro, K.S. Hydrogen peroxide modification enhances the ability of biochar (hydrochar) produced from hydrothermal carbonization of peanut hull to remove aqueous heavy metals: Batch and column tests. *Chem. Eng. J.* **2012**, *200–202*, 673–680. [[CrossRef](#)]
110. Víglašová, E.; Galamboš, M.; Danková, Z.; Krivosudský, L.; Lengauer, C.L.; Hood-Nowotny, R.; Soja, G.; Rompel, A.; Matík, M.; Briančin, J. Production, characterization and adsorption studies of bamboo-based biochar/montmorillonite composite for nitrate removal. *Waste Manag.* **2018**, *79*, 385–394. [[CrossRef](#)]

111. An, X.; Wu, Z.; Qin, H.; Liu, X.; He, Y.; Xu, X.; Li, T.; Yu, B. Integrated co-pyrolysis and coating for the synthesis of a new coated biochar-based fertilizer with enhanced slow-release performance. *J. Clean. Prod.* **2021**, *283*, 124642. [[CrossRef](#)]
112. An, X.; Wu, Z.; Liu, X.; Shi, W.; Tian, F.; Yu, B. A new class of biochar-based slow-release phosphorus fertilizers with high water retention based on integrated co-pyrolysis and co-polymerization. *Chemosphere* **2021**, *285*, 131481. [[CrossRef](#)] [[PubMed](#)]
113. Show, S.; Mukherjee, S.; Devi, M.S.; Karmakar, B.; Halder, G. Linear and non-linear analysis of Ibuprofen riddance efficacy by Terminalia catappa active biochar: Equilibrium, kinetics, safe disposal, reusability and cost estimation. *Process Saf. Environ. Prot.* **2021**, *147*, 942–964. [[CrossRef](#)]
114. Azalok, K.A.; Oladipo, A.A.; Gazi, M. UV-light-induced photocatalytic performance of reusable MnFe-LDO–biochar for tetracycline removal in water. *J. Photochem. Photobiol. A Chem.* **2021**, *405*, 112976. [[CrossRef](#)]
115. Lehmann, J.; Joseph, S. *Biochar for Environmental Management: Science and Technology*; Routledge: London, UK, 2009.

Disclaimer/Publisher’s Note: The statements, opinions and data contained in all publications are solely those of the individual author(s) and contributor(s) and not of MDPI and/or the editor(s). MDPI and/or the editor(s) disclaim responsibility for any injury to people or property resulting from any ideas, methods, instructions or products referred to in the content.